An Innovative Thermo-Electric Energy Harvesting Module for Asphalt Roadway

Project No. 20PUTSA42

Lead University: University of Texas at San Antonio

TECHNICAL DOCUMENTATION PAGE

1. Project No. 20PUTSA42	2. Government Accession No.	3. Recipient's Catalog No.	
4. Title and Subtitle An Innovative Thermo-Energy Harvesting Module for Asphalt Roadway Pavement		**5. Report Date** Oct. 2021	
		6. Performing Organization Code	
7. Author(s) Seyed Amid Tahami https://orcid.org/0000-0003-2100-8805 Samer Dessouky https://orcid.org/0000-0002-6799-6805		**8. Performing Organization Report No.**	
9. Performing Organization Name and Address Transportation Consortium of South-Central States (Tran-SET) University Transportation Center for Region 6 3319 Patrick F. Taylor Hall, Louisiana State University, Baton Rouge, LA 70803		**10. Work Unit No. (TRAIS)**	
		11. Contract or Grant No. 69A3551747106	
12. Sponsoring Agency Name and Address United States of America Department of Transportation Research and Innovative Technology Administration		**13. Type of Report and Period Covered** Final Research Report Sep. 2020 – Aug. 2021	
		14. Sponsoring Agency Code	
15. Supplementary Notes Report uploaded and accessible at: http://transet.lsu.edu/			

16. Abstract

The importance of green technologies for generating renewable energy and sustainable development is widely accepted. Road surfaces are exposed to solar radiation that generates thermal gradients and heat flow in the pavement layers. The heat stored can be harvested providing an untapped source of renewable energy. This report presents the design, construction, and assessment of an improved thermoelectric energy prototype for harvesting heat energy from roadway pavements. To accomplish this, various prototype designs were simulated using Finite Element (FE) analysis, followed by design construction and laboratory testing of the most promising prototypes to evaluate their power harvesting capabilities. The main design components of these prototypes are a heat collector/transfer plate, thermoelectric generators (TEG), and a cooling module consisting of a heat sink, phase change material, and an insulation box. The results suggest a direct relationship between thermal gradients and power generation and point out the importance of the cooling module in maintaining the efficiency of the harvester. An optimum harvester design would generate an average power output of 29 mWatt or 835 J over 8 hours per day in South Texas. Extrapolating this output for an installation that covers a length of 1 kilometer of a roadway could produce an average of 23.2 kWh/day, which appears to be a promising independent source of power for roadside signage and sensors.

17. Key Words Energy Harvesting, Thermoelectric, Pavement		**18. Distribution Statement** No restrictions.	
19. Security Classif. (of this report) Unclassified	**20. Security Classif. (of this page)** Unclassified	**21. No. of Pages** 44	**22. Price**

Form DOT F 1700.7 (8-72) authorized.   **Reproduction of completed page**

SI* (MODERN METRIC) CONVERSION FACTORS

APPROXIMATE CONVERSIONS TO SI UNITS

Symbol	When You Know	Multiply By	To Find	Symbol
LENGTH				
in	inches	25.4	millimeters	mm
ft	feet	0.305	meters	m
yd	yards	0.914	meters	m
mi	miles	1.61	kilometers	km
AREA				
in^2	square inches	645.2	square millimeters	mm^2
ft^2	square feet	0.093	square meters	m^2
yd^2	square yard	0.836	square meters	m^2
ac	acres	0.405	hectares	ha
mi^2	square miles	2.59	square kilometers	km^2
VOLUME				
fl oz	fluid ounces	29.57	milliliters	mL
gal	gallons	3.785	liters	L
ft^3	cubic feet	0.028	cubic meters	m^3
yd^3	cubic yards	0.765	cubic meters	m^3
NOTE: volumes greater than 1000 L shall be shown in m^3				
MASS				
oz	ounces	28.35	grams	g
lb	pounds	0.454	kilograms	kg
T	short tons (2000 lb)	0.907	megagrams (or "metric ton")	Mg (or "t")
TEMPERATURE (exact degrees)				
^{o}F	Fahrenheit	5 (F-32)/9 or (F-32)/1.8	Celsius	^{o}C
ILLUMINATION				
fc	foot-candles	10.76	lux	lx
fl	foot-Lamberts	3.426	candela/m^2	cd/m^2
FORCE and PRESSURE or STRESS				
lbf	poundforce	4.45	newtons	N
lbf/in^2	poundforce per square inch	6.89	kilopascals	kPa

APPROXIMATE CONVERSIONS FROM SI UNITS

Symbol	When You Know	Multiply By	To Find	Symbol
LENGTH				
mm	millimeters	0.039	inches	in
m	meters	3.28	feet	ft
m	meters	1.09	yards	yd
km	kilometers	0.621	miles	mi
AREA				
mm^2	square millimeters	0.0016	square inches	in^2
m^2	square meters	10.764	square feet	ft^2
m^2	square meters	1.195	square yards	yd^2
ha	hectares	2.47	acres	ac
km^2	square kilometers	0.386	square miles	mi^2
VOLUME				
mL	milliliters	0.034	fluid ounces	fl oz
L	liters	0.264	gallons	gal
m^3	cubic meters	35.314	cubic feet	ft^3
m^3	cubic meters	1.307	cubic yards	yd^3
MASS				
g	grams	0.035	ounces	oz
kg	kilograms	2.202	pounds	lb
Mg (or "t")	megagrams (or "metric ton")	1.103	short tons (2000 lb)	T
TEMPERATURE (exact degrees)				
^{o}C	Celsius	1.8C+32	Fahrenheit	^{o}F
ILLUMINATION				
lx	lux	0.0929	foot-candles	fc
cd/m^2	candela/m^2	0.2919	foot-Lamberts	fl
FORCE and PRESSURE or STRESS				
N	newtons	0.225	poundforce	lbf
kPa	kilopascals	0.145	poundforce per square inch	lbf/in^2

TABLE OF CONTENTS

LIST OF FIGURES

LIST OF TABLES

ACRONYMS, ABBREVIATIONS, AND SYMBOLS

AADT   Annual Average Daily Traffic

FHWA   Federal Highway Administration

TxDOT   Texas Department of Transportation

USDOT   United States Department of Transportation

EXECUTIVE SUMMARY

Securing renewable energy sources is essential for long-term environmental sustainability. The depletion of fossil fuels and the adverse effects of their combustion create an urgent need for the advent of alternative green energy sources. Harvesting energy from asphalt pavements has shown promise in generating green electrical energy. Asphalt pavements are one of the most prominent components of civil engineering infrastructure. In the United States alone, they extent to over 6 million lane-km. Tapping into the energy stored in them has been the subject of several recent research efforts. The harvested energy can have multiple potential applications including powering pavement health monitoring devices, road-side or traffic lights, infrastructure sensors, and near-field communication systems. Therefore, there is a considerable research interest and effort to effectively harvest energy from pavements as supported by several studies recently been conducted to assess the feasibility of using roadways to generate green energy. One of these studies are to harvest thermal energy from asphalt pavement using thermoelectric generators (TEGs) inside the pavement structure. Solar radiation absorbed by pavement surface causes temperature gradient which can be converted into electric energy by TEG. TEG can convert heat into electrical energy based on the Seebeck effect. Using TEGs offers several benefits such as environmentally friendly energy, no moving mechanical components and low maintenance requirements. In this report, the researchers optimized their original design to improve efficiency and longevity in the material choice, fabrication and dimensions. To accomplish this, various prototype designs were simulated using Finite Element (FE) analysis, followed by design construction and laboratory testing of the most promising prototypes to evaluate their power harvesting capabilities. The main design components of these prototypes are a heat collector/transfer plate, TEG, and a cooling module consisting of a heat sink, phase change material, and an insulation box. The results suggest a direct relationship between thermal gradients and power generation and point out the importance of the cooling module in maintaining the efficiency of the harvester. An optimum harvester design would generate an average power output of 29 mWatt or 835 J over 8 hours per day in South Texas. Extrapolating this output for an installation that covers a length of 1 kilometer of a roadway could produce an average of 23.2 kWh/day, which appears to be a promising independent source of power for roadside signage and sensors.

1. INTRODUCTION

Population growth and rising living standards have dramatically increased worldwide energy needs. Reliance on fossil fuels for generating this energy has undesirable environmental consequences (1-2). The United States Department of Energy (US DOE) reports that the world energy consumption is anticipated to rise by 44% from 2006 to 2030 (3). Although non-renewable fossil fuels supply 80% of the requirements of energy, this type of energy is about to be exhausted. Therefore, finding alternative energy sources is critical in providing a sustainable future (4). Recently, renewable energy sources have attracted significant attention due to their social acceptance and capability of supplying sustainable energy (5). Harvesting renewable energy has practically no adverse environmental impacts compared to the traditional processes used for extracting fossil fuels. Furthermore, using renewable energy has considerable environmental benefits, including a reduction in harmful emissions of carbon monoxide (CO), nitrogen oxides (NOx), and sulfur dioxide (SO_2) (6).

Roadways play a fundamental role in the worldwide transportation system. For instance, the US and China transportation systems consist of about 6.0 and 4.7 million center-line kilometers of paved roadways, respectively (1, 7). These roadway pavements are continuously exposed to solar energy and absorb heat. Harvesting this heat can provide an untapped source of renewable energy (8).

The importance of green technologies for generating renewable energy and sustainable development is widely accepted. Road surfaces are exposed to solar radiation that generates thermal gradients and heat flow in the pavement layers. The heat stored can be harvested providing an untapped source of renewable energy. This paper presents the design, construction, and assessment of an improved thermoelectric energy system prototype for harvesting heat energy from roadway pavements. To accomplish this, various prototype designs were simulated using Finite Element (FE) analysis, followed by design construction and laboratory testing of the most promising prototypes to evaluate their power harvesting capabilities. The main design components of these prototypes are a heat collector/transfer plate, thermoelectric generators (TEG), and a cooling module consisting of a heat sink, phase change material, and an insulation box. The results suggest a direct relationship between thermal gradients and power generation and point out the importance of the cooling module in maintaining the efficiency of the harvester. An optimum harvester design can produce on average a power output of 29 mW over a period of 8 hours of summer sunshine in South Texas. Extrapolating this output for an installation that covers a length of one kilometer of a roadway could produce an average of 32.2 kWh/day which appears to be a promising independent source of power for roadside signage and sensors.

2. OBJECTIVES

- Introduce the thermoelectric energy harvester system that aims to produce electrical power from unused thermal energy available in regular asphalt pavements.
- Examine different designs of the system under field-simulated conditions in the laboratory
- Examine the systems with simulated field conditions using Finite Element analysis

3. LITERATURE REVIEW

3.1. Introduction

The concept of energy conservation and the need for developing alternative energy resources has become pressing due to the environmental impact of fossil fuels. The massive accumulation and generation of greenhouse gases is altering the Earth's climate, while conventional energy sources are non-renewable and being depleted. Consequently, the search for environmental-friendly, low-cost energy resources becomes increasingly necessary (9-11).

Energy harvesting (scavenging) is a process that captures unused ambient energy that would otherwise be lost in the form of heat, light, sound, vibration, stress or movement. The United States transportation system consists of about 6 million kilometers of roadways. These roadways are exposed to energy from vehicle vibrations, traffic loading strains, and thermal gradients that can be harnessed. These resources can be potentially converted into usable energy such as electric power. Capturing this unused energy is the challenging aspect of the harvesting process. Successful energy harvesting from highway pavements can lead to sustainable transportation infrastructure systems.

Energy harvesting technology can be used to overcome growing challenges facing the Texas Department of Transportation (TxDOT) as demand for services stretches further from an efficient and reliable source of revenue. This imbalance is in part, catalyzed by Texas's rapidly growing population. This population growth places tremendous strain on TxDOT's mission to provide better transportation services. Gas tax revenues have long provided TxDOT with the supporting revenue. However, gas tax revenues are declining and are becoming less dependable, as electric vehicles absorb a larger percentage of the automobile market share and as vehicles become more fuel efficient. Thus, the opportunity of energy harvesting from road infrastructure provides TxDOT a possible alternative financial resource that could supplement conventional fuel tax income. **Error! Reference source not found.** depicts the projected disproportionately increasing rates in available roadway lane-miles, population, and vehicle-miles travelled. Clearly, there will be a growing gap between transportation infrastructure demand and supply.
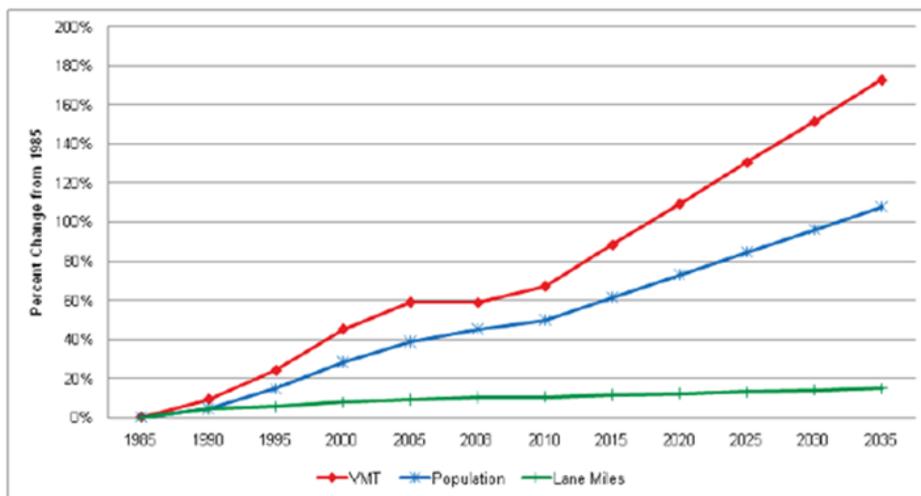
Figure 0. Lane Miles, Population, and VMT Percent Change over 50 Years

A major and declining financial resource for the construction and maintenance of roadway infrastructure is the State fuel tax of 20 cents/gal. As vehicles become more fuel efficient, as more electric (i.e., plug-in) vehicles are introduced, and as an increasing population demands the building of more lane miles, roadways will suffer great deterioration if not properly funded and maintained. **Error! Reference source not found.** depicts the trend of increasing sales of electrical vehicles. Every electric vehicle generates vehicle miles traveled without contributing to roadway taxes. Texas roads are continuously subject to vibrations, impact, solar heat, and repeated strains. Upon these roadways, the mechanical energy of millions of passing vehicles is left untapped and wasted. Harvesting and transforming these energy into electric power can potentially be stored in roadside batteries, fed directly into the grid, recharge electric cars, power monitoring sensors, and illuminate traffic lights. This will lead to a sustainable roadways infrastructure system that can offset the financial cost of maintaining these roadways.
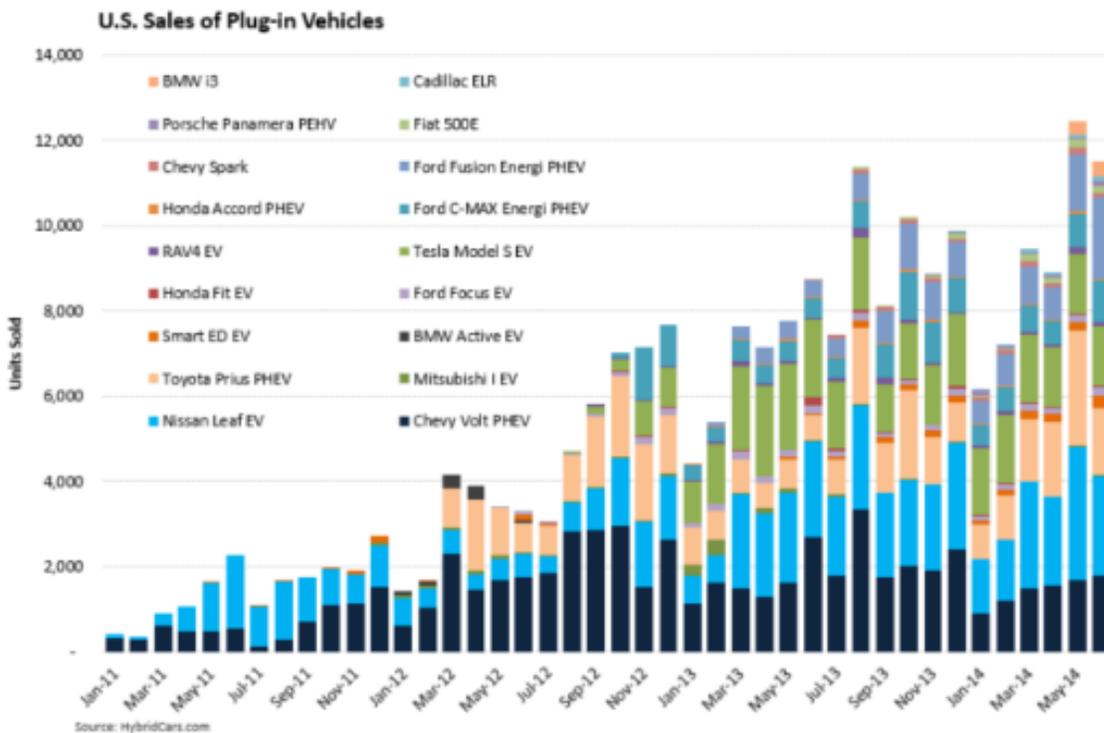
Figure 0. The increase rate of U.S. Sales of Plug-in Vehicles over a period of three Years (12)

The objective of this chapter is to present some of the current technologies and conceptual approaches to harvest energy from infrastructure, in particular asphalt pavement roadways. These include, solar roadways, solar collector systems, Photovoltaic, thermal gradient devices, and piezoelectric materials.

3.1.1. Existing Energy Harvesting Technologies

Technologies and techniques available for the energy harvesting process include thermoelectricity, solar radiation, ocean currents, wind energy, and mechanical motions. Some of these technologies are commercially available, while others are still in the development stage. Storage of the energy harvested is another technical challenge, which needs to be resolved in order to prove the feasibility of the harvesting process. Examples of commonly available energy sources include:

- Solar energy using photovoltaic (PV) cells. The PV cells convert light energy from solar radiation into electrical energy. However, PV systems are highly dependent upon tilting angle, exposure durations, and exposure intensities.

- Thermal energy from roadway surfaces, heaters, and human body using thermoelectric generators (TEG). The TEGs consist of thin thermocouples in a configuration capable of exploiting temperature gradients a low as 2 degrees Celsius. These gradients can occur between interfaces such as skin to air and ground to air. This technology has been used for homeland defense (to detect high skin/body temperatures), energy harvesting, and agricultural management.

- Electromagnetic energy using transformers, inductors, and coils. This technology utilizes a magnetic field to convert mechanical energy into electrical energy. An oscillating mass attached to a coil passes through a magnetic field thus producing electric energy. The coil passes through a magnetic flux, inducing a voltage in accordance with Faradays' Law.

- Mechanical energy in the form of vibrations, strain, mechanical stress, pressure, and rotations. One method of capturing mechanical energy is with piezoelectric materials. Piezoelectric materials are transducers that generate electric energy when mechanically deformed or strained but can also generate mechanical vibrations when exposed to an electric potential.

Error! Reference source not found. shows a comparison between the aforementioned harvesting technologies and their power densities. Power density is the amount of power stored within a given unit of mass or region of space per unit volume. The figure relates power density per unit volume with various energy harvesting methods including variable illumination states for PV materials (13). As shown in the figure, the PV cell is one of the highly effective to power producer particularly in peak hours among the other technologies. More details on existing harvesting technologies on roadways are explained in the next sections.
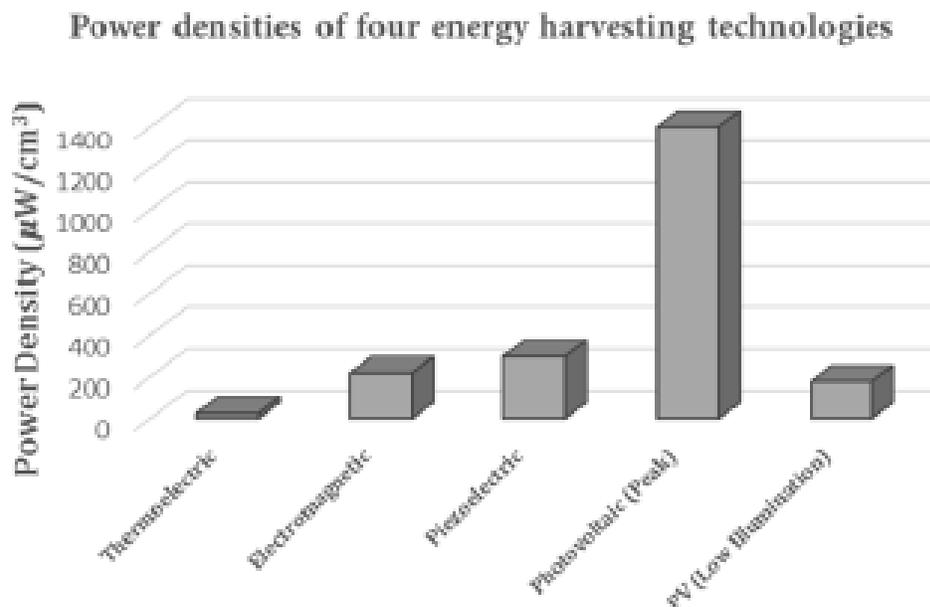
Figure 3. Power Density of Various Energy Harvesting Methods (13)

3.1.2. Asphalt Solar Collector Combined with Piping System

The temperature of asphalt pavement increases throughout the day due to the absorption of solar radiation. The materials incorporated into asphalt pavement have the property of high absorptivity coupled with low conductivity. These characteristics along with the high thermal capacity means that pavements can reach a very high temperature, even higher than the temperature of the surrounding air. This characteristic makes asphalt pavement an attractive source for potential energy harvesting. Also, when the temperature rises significantly, the asphalt can cause what is known as an urban heat island effect (27-28). This can lead to high ambient air temperatures and thus deteriorating air quality. The asphalt solar collector (ASC) concept involves a piping system within the pavement layers to conduct heat through an appropriate fluid. Heat from this fluid can be transferred and stored to insulated chambers and used for a variety of purposes such as anaerobic digesters, deicing or domestic uses (29). **Error! Reference source not found.** shows an example of an ASC installation in Holland during construction. A positive side effect of ASC systems is that they reduce the temperature in the asphalt pavement and hence reduce heat island effects during the summer.

Figure 4. Asphalt solar collector system under construction on a bridge in Rotterdam (14)

In 2007, Liu et al. analyzed the snow-melting process on a heated pavement surface using a numerical model involving a hydronic energy harvesting system. They studied the heat fluidity of the pavement surface under different environmental conditions and predicted the corresponding pavement surface temperatures. The modeling of this hydronic heat system in a bridge deck (**Error! Reference source not found.**), illustrated that the required time for pre-heating the bridge and the distance between water pipes are two significant factors affecting the snow melting performance and the maximum fluid temperature. They suggested that the required heating system capacity, the fluid temperature and the density of the embedded piping system are the primary criteria in designing an effective pavement energy harvesting system.
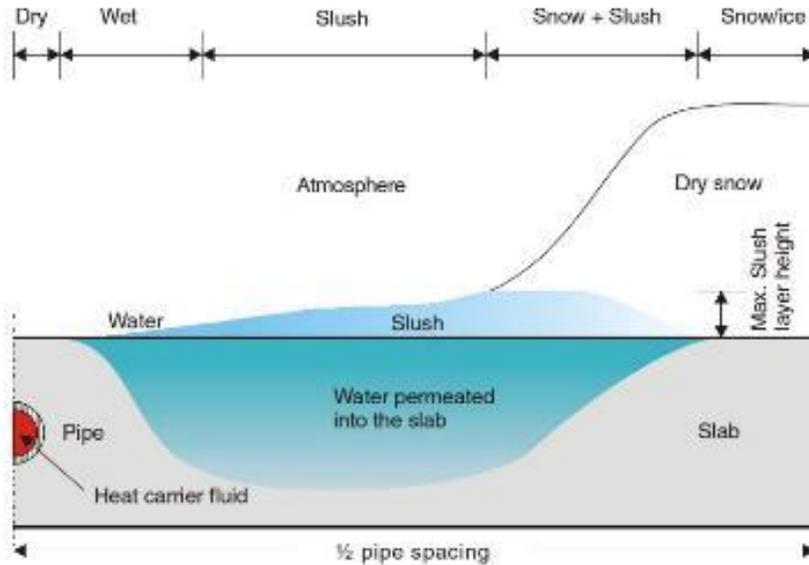
Figure 5. Variation of surface condition on a heated pavement slab during the snow melting process (15).

Similarly, Dawson et al. (2011) developed a "Thermally Optimized Pavement" using pipes installed at two positions in the pavement. To improve hydronic performance, they suggested embedding the pipes close to the pavement surface, and install a low-grade heat source and a heat-sink at bottom of the pavement to improve performance during the winter and the summer months, respectively (16). Another study performed by Gao et al. (2010) demonstrated a roadway ice-snow melting system. As shown in **Error! Reference source not found.**, the system was combined with a "Slab Solar Connection" containing a series of embedded pipes and underground thermal energy storage. The results showed that, higher flow rate and denser pipe arrangement increased the effectiveness of this energy harvesting system. Also, they found that wind speed, ambient temperature, and solar radiation are other important factors. When they increased the flow rate in the pipes, the effective time of collecting the heat from the fluid in the pipes decreased. They concluded that an arrangement of closely-spaced pipes achieves 42% heat collecting efficiency (17).
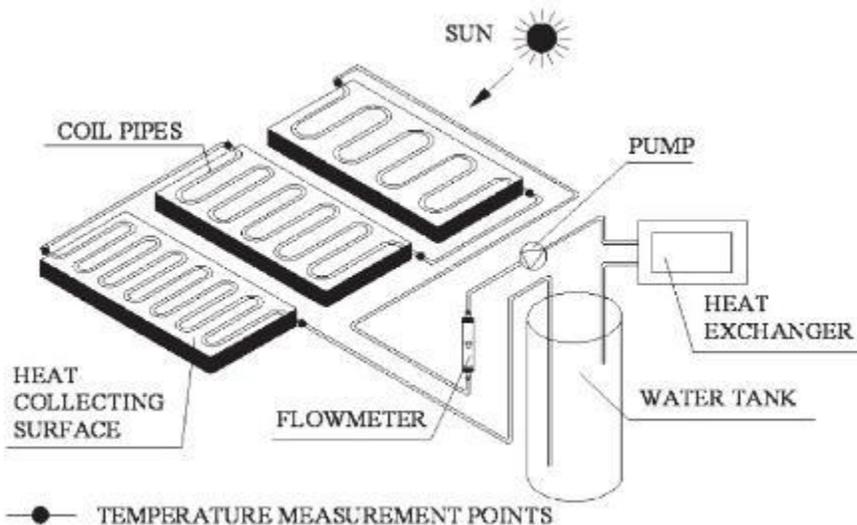
In an attempt to build an efficient solar collector system for pavements (9), researchers studied the effects of temperature, rate and inlet water flow, and pipe arrangement on heat conduction, convention, and radiation (**Error! Reference source not found.**). The researchers concluded that the diameter of the pipes is the most significant factor influencing the temperature distribution and cooling effect. Also, they found that the flow rate of the fluid that moves inside the pipes does not have considerable effect on the temperature of the pavement and surrounding area. As a result, the larger pipe diameter gave steeper temperature differences between the pipe and the pavement surface, therefore it made the water cooler and led to lowering the temperature at the surface of the pavement (9-10).

Work by Wu et al. (2011) suggested that "*Thermal collection starts as long as the temperature at the location of the pipes reaches the balance temperature needed for specific heat transfer flow rate, wind speed, irradiation intensity and other conditions*". Since the top surface of the cooled pavement has a lower temperature, it might increase the pavement stiffness and improve its resistance against deformation in hot climates, and consequently results in a longer life. Overall, in order to harvest energy from the pavement along with decreasing urban heat island effects, the interactions among pavement thickness, weather conditions, albedo effect, and type of the materials should be considered carefully (29).
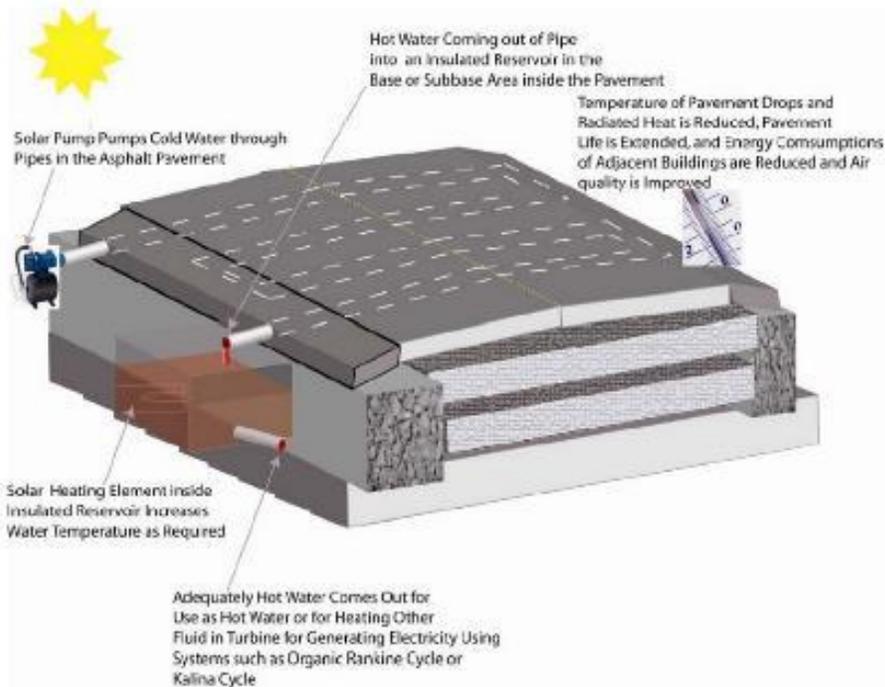
Figure7. Concept of harvesting energy from pavements and reducing pavement temperature, (9)

3.1.3. Sound Barrier PV Panels

Sound walls, or noise barriers, are exterior structures designed to shield inhabitants located in sensitive land use areas from noise pollution. These structures are commonly found running parallel to roadways, railways, and airports. For roadways, the sounds are generated by vehicle aerodynamics, vehicle engines, and tire noise which vary in intensity with speed. These barriers are usually constructed with concrete, steel, and/or masonry. Such structural materials can easily be designed to support the additional loading of photovoltaic (PV) panels for energy harvesting. PV panels convert solar radiation into direct electric current using semi-conductors and the photoelectric effect. The photoelectric effect occurs when photons are absorbed by semiconducting materials like silicon when sunlight strikes a photovoltaic material. The energy from the photons knocks electrons loose and allows them to flow in a current in the presence of an electric field. The electric field is created by the separation of charge carriers. This energy harvesting method employs composite solar panels of PV material. PV materials include mono-crystalline silicon, amorphous cells, cadmium telluride, and polycrystalline silicon. **Error! Reference source not found.** shows various PV noise barrier configurations. Configurations include conventional and state-of-the-art ideas. For example, the N-S vertical bifacial configuration is a PV-module that is light sensitive on both sides and simultaneously acts as a noise reflective element (18). Additionally, the PV modules can be placed on the opposite side of the sound barrier and does not have to face the road.
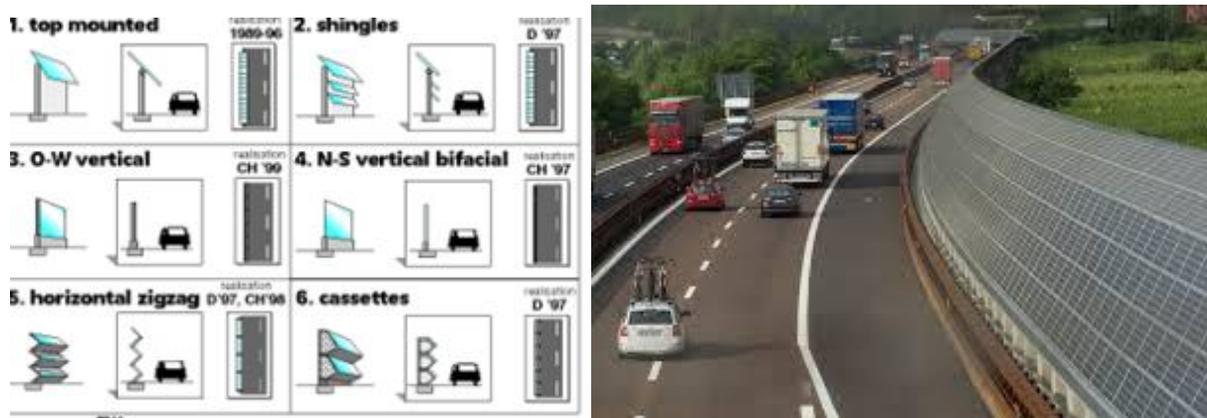
Figure 1. Various PV Noise Barriers Configurations (18)

In 1989, the first PV noise barrier was a 100 kW strip installed along the A13 highway in Switzerland (**Error! Reference source not found.**). The Swiss National Energy Research with the cooperation of the German Federal Ministry of Education, Science, Research and Technology funded this PV installation to investigate its application in roadways. This installation has proven to be highly efficient with low maintenance. The glass surface has never been cleaned but has had no significant degradation of the array efficiency (19) without any major interruptions for 10 years. In another study performed by Nordman et al. (2000) summarized the capability of electricity production from existing PV sound barriers technologies from six European countries. The researchers highlighted that the existing technologies are able to potentially produce 800 MWp which is about 680 GWh electrical energy per year in those six countries. To achieve that purpose, it was suggested to plan and design the noise barrier and PV plant simultaneously as a single project with close cooperation of PV and sound experts (18). In 2007, Grasselli et al. tested six

different PV sound barrier for road application to evaluate their energy performance and acoustical functioning. They investigated motorist safety in case of crashes, appropriate plant construction, long-term performance, and acoustic functioning. The researchers concluded that PV systems require maintenance. Also, the results showed that the overheating of PV and the pollution produced by vehicles should be considered over the life of these systems (20).

Figure 9. Photovoltaic noise barrier along the A13 highway in Switzerland (20).

The PV sound barrier efficiency is highly dependent upon panel tilt angle (21). This is done to maximize solar collection but also dependent upon the direction of the roadway to serve as a noise barrier. For this reason, the optimal placement of solar panels on sound barriers are likely to be along roads in an east-west direction so to gather solar radiation throughout the day by tilting the PV cells continuously. However, investment into a universal mounting system may further expand the potential miles of roadways available for mounting solar panels. The solar panels should also be placed at a height sufficient to limit contamination from soil and road debris, (21).

The PV (solar) technology is well established and ready for implementation in either self-standing roadside installations or as part of sound barrier systems. The drawback of stand-alone installations is that they require considerable roadside real estate, which makes them less attractive in urban areas. Unfortunately, there is an inverse relation between areas of available real estate and energy demand. Urban areas have a much greater energy demand, yet have less space available for the installation of solar panels than rural areas.

3.1.4. Solar Roadways

As described already, solar energy is one of the most relevant and readily applicable energy harvesting method to integrate into the roadway infrastructure. A variation of PV installation technologies described above is imbedding it directly onto the highway infrastructure surface. That is, make PV panes the driving surface of the roadway. There have been several efforts to this end.

In 2006, Solar Roadways Inc. designed and developed solar panels for roadways and built a parking lot covered by solar panels. The developed solar roadway panels are equipped with integrated heating component that maintain a temperature above freezing. This helps the roads to be free of snow, and ice during cold seasons (**Error! Reference source not found.**). There are also

Figure 10. Solar panel modular (22)

LED lights embedded in the panels that can highlight edge-lines and signage on the road. Taking advantage of the LED lights could be eliminate the needs for painting and marking the roads. The company claims that it can produce more than 698 Megawatt-hours from one mile square of covered solar panels in one year (22).

Figure 11. Solar bike lane in the Netherland (22).

In a similar attempt in the Netherland, the engineers of SolaRoad installed solar panels in a 230-feet bike lane (**Error! Reference source not found.**). The fragile parts were encased in thick glass layers to be able to withstand the heavy loads caused by traffic. SolaRoad claims that the output power during the first six months is around 3 megawatt-hours which is approximately equal to the amount of electricity required for a single occupancy house for one year.

In 2010, researchers in South Korea (23) utilized PV cells inside the pavement. Recognizing the strength limitations of conventional PV panels, they tried to develop appropriate cells to bear the traffic loads. They investigated the feasibility of PV technologies as a harvest energy system in roadway pavements by developing thin solar cells that can properly function and meet roadway conditions.

A problem facing solar roadways, regardless of the installation technique is the effect of shading or partial shadowing. This is usually caused by obstructions such as from buildings, trees, and cloudy conditions. However, a solar roadway experiences additional shading from passing vehicles. The two most important factors for computing the reduction on PV panel efficiency from vehicle shading is their number, type (i.e., it defines their length) and their speed (24). There are also fluctuations in energy output due to variations in temperature. Optimal temperature for solar panel efficiency is around 25 degrees Celsius and with every 1 degree increase in the temperature, there is a 0.44% decrease in maximum power output (24).

Another reason of efficiency loss is soiling of the surface (particulate accumulation). Energy losses from soiling typically range between 5 and 15% (24). Frequently traveled solar roadways would have the potential of accumulating a heavy amount of particulate material making soiling a serious concern. Tilting angles must also be considered for solar roadways. Tilting angle effects are the losses of energy output due to the directional travel of solar rays being less than perpendicular relative to the surface of the solar panel. Obviously, solar highways have a fixed titling angle affecting their efficiency throughout the day.

Another technical issue is the solar panel resilience to traffic loads, while providing sufficient friction. Current solar panel surfaces are designed to resist loads from hail impact and accumulated snow. Handling vehicular loads poses unique and conflicting structural requirements for the glass that encases PV panels, in terms of their thickness, composition and surface texture. As the thickness of the material increases, their structural integrity increases but their light transmissivity decreases. The type of material chosen affects light absorption, strength, and cost. Glass can theoretically be designed to have very high structural strength, however it must be manufactured without flaws to allow high light transmissivity. Providing surface texture could negatively affect translucence and absorption capabilities.

A more conservative approach of integrating PV technology harvesting in the transportation infrastructure is their installation on top of covered parking areas. In 2007, Golden et al. recommended the use of PV cells on parking canopies to decrease the urban heat island effect in those areas, while generating electric power. Decreasing pavement temperature results in lowering aging, improving resistance to cracking, and extending pavement life (25). Another successful canopy PV installation was on Blackfriars Railway Bridge in London, where 4,400 solar panels were installed over railway tracks. The anticipated electricity output of this system is about 900 MWh yearly, which will result in a reduction of 500 tons of carbon emissions (21).

A variation of this approach was described by Strauss et al. (2009), whereby flexible PV panels were installed directly over long-term parked vehicles (e.g., school buses) to generate electrical power. They named this concept 'Vehicle Surfaces Parking Lot PV Solar Energy Power Generation System'. The generated electric power can be used to either run small appliances (e.g., AC systems to cool the parked vehicles or be converted to AC current and be fed into the electric network. The results suggested that such temporary PV arrays could provide sufficient power to electrify several nearby buildings (26).

3.1.5. Piezoelectric Energy Harvester Systems

The movement of vehicles on pavements is a form of kinetic energy. A portion of this energy is transferred into the pavement in the form of vibrations, strains, and compression forces. Energy is transferred mainly through the impact of the vehicle weight on pavement through the tires. There are roughly a quarter of a billion vehicles registered in the United States. These vehicles impose great kinetic and strain energy through vibrations and traffic loading strains over the life of pavements. This energy could be potentially captured and converted to usable electric power. This energy can be harvested using piezoelectric transducers (PZT) (30- 31). The PZT are capable of generate electric voltage due to the application of loading stresses and vibrations. PZT has the special property of generating an electric voltage when subjected to deformation by dimensional alteration or vibration.

Xiong et al. (2014) at Virginia Tech tested nine energy harvesters in the field and laboratory. They installed some of their energy harvesters in the field and tested them for 18 months. There are typically two different coupling modes which are 33-mode and 31-mode. To generate energy under a 33-mode, the piezoelectric material must be displaced along the poling direction. To generate energy under a 31-mode, the piezoelectric material requires transverse displacement. The choice was made to install the piezoelectric elements 3 inches below the surface and it was found through stresses analysis that the 33-mode was preferable to the 31-mode, which was too heavily dependent on vehicle speed. The 33-mode was preferable because its power output was directly proportional to the stress applied to it. Different interfacial circuits were designed to optimize the energy gathering from the piezoelectric harvester. Analysis was conducted to minimize stress concentration on the piezoelectric material through increasing surface area using many piezoelectric discs and changing the materials geometry to circular shape rather than a rectangular shape. The energy harvesters were installed in three locations including a weigh station without affecting traffic and the adjacent pavement. **Error! Reference source not found.**2 depicts the placement of eight energy harvesters beneath the pavement for the weigh station approximately on the wheel path of the bypass lane. Epoxy was applied in the pits to promote bonding and to the right of the image shows the straight line trenches for conduit housing the electric cables (32).

Figure 12. The prototype and pattern of In-situ Energy Harvester Placement (32)

3.1.6. Thermoelectric Energy Harvesting

The top surface of pavement has characteristics that make it absorb sunlight energy and store it. The temperature of a pavement structure varies along the pavement layers so that the temperature at the surface is higher and decreases with depth. A thermal gradient of variable magnitude exists between the pavement base and the subgrade throughout the day. This thermal gradient can be used to actuate thermoelectric materials to generate electric power (33). The efficiency of a thermoelectric system highly depends on the electric conductivity of the device, the thermal conductivity, the seebeck coefficient (i.e., a measure of the induced thermoelectric voltage in response to a temperature difference across that material), and the thermal gradient. The produced energy can be used to supply power for advanced sensors with applications in the transportation area such as pavement health monitoring (29).

Among all energy harvesting techniques, the application of thermoelectric generators (TEGs) for generating electrical energy from pavement has been developed in recent years and looks promising. The TEG device is able to directly convert thermal energy into electricity according to the Seebeck effect, and it has exhibited great potential in the case of waste heat recovery. The application of TEGs delivers several advantages, such as being environmentally friendly, having long-term durability, having no moving mechanical components, and requiring low maintenance (34). The asphalt pavement is continuously exposed to solar radiation that can heat the pavement up to 70˚C due to the high absorptivity of its black materials. This source of energy, heretofore unused, has attracted attention as a potentially renewable and clean energy source.

In 2006, Hasebe et al. designed and tested the TEG using heat extracted by a piping system incorporated into the pavement. The hot temperature of the TEG's side was supplied by hot water circulating inside the heating pipe. A cooling pipe cooled by river water connected to the cold side of the TEG, which induced a temperature difference across the TEG's sides and eventually produced electrical power (35).

In 2012, Wu and Yu studied the TEG system to generate electrical power from the heat from pavement. They proposed that one side of the TEG be attached to an aluminum plate embedded under the pavement and the other side connected to an aluminum rod placed into the subgrade to facilitate the cooling process and thus increase electrical energy production (29).

In 2015, researchers at the University of Chang in China studied the efficiency of the thermoelectric energy harvester in the lab. They fabricated asphalt specimens, which were heated up to 70°C by lamp to simulate solar radiation. The TEG modules were inserted into the specimen at different depths, and it was found that, with respect to system efficiency and different temperature gradients, the optimal depth was 2-3 cm under the pavement surface. Furthermore, the inserted TEGs inside the specimens were subjected to a dynamic stability test, and it was confirmed that the TEG harvester had proper durability at a depth of 2 cm (33).

In 2017, Datta et al. assessed a prototype of a thermoelectric energy harvesting system using finite element analysis and laboratory and field testing. A Z-shape copper plate was embedded under the asphalt pavement to capture the heat from the pavement and carry it to the bottom, where the hot side of the TEGs were attached, and the cold sides of the TEGs were connected to the aluminum heat sink filled with soil. The proposed system was capable of producing an average of 10 mWatt over 8 hr (36).

Jiang et al. designed an enhanced TEG system composed of a rectangular aluminum heat-conduction plate, a thermoelectric device, and a cold-end module. The aluminum plate's role was to extract the heat and transfer it to the TEGs. Also, in the cold-end module, a water tank covered by a shading board was used to apply low temperature (37).

The literature showed that previous studies explored a variety of strategies to improve the system efficiency by suppling more heat for the hot side of the TEG and providing lower temperature for the cold side of the TEG; however, some essential and influential factors should be considered for efficiency improvement. For instance, the heat exchangers, like the aluminum chamber, copper plate and aluminum bar, were not properly insulated (causing heat loss), and the coolant modules could not keep the temperature on the cold side of the TEG down for two reasons: a) a lack of insulation between the coolant module and the surrounding area; and b) the heat sinks were filled with soil or water, which have low thermal storage capacity.

Although the application of pavement thermoelectric technology is feasible, published studies on this topic appear to be limited. Thus, the implementation of TEG technology in pavement is still in the early stages, and further research is required to enhance the design and increase the efficiency of the TEG harvester system. This study fills the research gap and evaluates and optimizes the performance of the thermometric-based pavement system. The paper describes the configuration, modeling and laboratory experiments. In order to assess different parameters affecting the performance of the system, the effect of the TEG size (i.e., 4 cm x 4 cm and 6.4 cm x 6.4 cm), the number of TEG devices (i.e. 1-4 modules), and pavement temperature (i.e., 45˚C to 65˚C) were studied. In addition, it presents an economic analysis of the power output of system. Findings of this study could help progress thermoelectric technology applications in pavements with perspective of energy sustainability.

In the research carried out by Wu et al., the application of TEGs for production of electrical energy in pavement was investigated. They showed that the temperature difference between the pavement surface and the surrounding soil (deep inside the ground) can be utilized to generate electricity. In this study, one side of the TEG device was attached directly to asphalt concrete layer and the other was attached to a plate embedded into the soil. This type of design, however, exposes the TEG to traffic loads, which may compromise their longevity (29). Wu et al. developed thermoelectric energy harvest system, in which one side of TEG connected to aluminum plate and the other side contacted with aluminum to generate power from thermal gradient between pavement and subgrade soil. The output power was about 0.05 mW that could be used to supply power of LED light (38). Liang and Li in 2015 at Chang'an University of China conducted a research to generate energy from asphalt pavement by using thermoelectric generator. By inserting TEG module in different depths within asphalt samples, durability and optimal location of module were investigated. The results indicated that the module could have the highest efficiency in depth of 20 mm-30 mm below the surface and the TEG module showed proper durability at the depth of 20 mm (33).

Generally, the amount of electricity generated from TEGs is mainly determined by the temperature gradients between hot and cold sides. TEG harvester designs must take advantage of this thermal gradient and maintain it over time, that is, provide an efficient cooling mechanism for delivering cold temperature at cold side of TEG can affect greatly the efficiency of system (40).

4. METHODOLOGY

4.1. Introduction

As presented in the literature review chapter, one of the approaches to harvest heat energy from asphalt pavement is the installation of thermoelectric generators (TEGs) inside the pavement structure. Solar radiation absorbed by pavement surface causes temperature gradient which can be converted into electric energy by TEG. TEG can convert heat into electrical energy based on the Seebeck effect. Using TEGs offers several benefits such as environmentally friendly energy, no moving mechanical components and low maintenance requirements (34).

4.2. Objective

The cooling system can play a critical role in increasing the efficiency of thermoelectric energy harvesters. Lower temperature at the cold side of TEG module can maximize the power output. In previous studies (36, 37, 39) the applied methods of cooling did not effectively reduce the temperature of the cold side of TEG. For instance, the utilized coolant modules without any proper insulation, were directly in contact with the surrounding area (e.g. soil and air).Direct contact with surrounding environment reduces the externally applied thermal gradient which might have significantly influenced the module and imposed the module to reach surrounding temperature in unfavorable way.

This chapter focuses on designing novel energy harvest system to enhance the efficiency of thermoelectric pavement structure by optimizing the heat transfer mechanism and proposing an innovative cooling technique consisting of heat sink, insulation box and phase change material (PCM). This chapter presents an optimized version of the earlier Z-shaped TEG prototypes (36).

4.3. Theoretical Background

The principle of TEG is based on the semiconductor TEG effect, which is known as the Seebeck/Peltier/Thomson effect, hence referred simply as Seebeck effect. This effect manifests itself as a voltage differential between the hot and cold site of a semiconductor in response to a thermal gradient (34). A thermoelectric module is typically composed of n- and p-type legs, providing the ability for electrons to move freely through metals and semiconductors (49). Voltage value is given by the following equation (41):

$$V = \alpha(T_h - T_c) \tag{1}$$

where:

V = the voltage of the TEG;

T_h = the hot side temperature of the TEG;

T_c = the cold side temperature of the TEG; and

α = the Seebeck coefficient of the TEG.

In addition, the current, electrical power and the total amount of heat can be obtained using the following equations (41, 42):

$$I = V/(R + R_l) \tag{2}$$

$$P = Q_h - Q_c = I^2 R_l \qquad [3]$$

$$Q = \alpha I T_c + K(T_h - T_c) - 1/2 I^2 R_L \qquad [4]$$

where:

I = the current;

R = the internal resistance of TEG;

RL = the Load resistance;

(Qh – Qc) = the heat flux due to temperature gradient;

Q = the total quantity of heat, and K is the heat transfer coefficient.

4.4. Design Concept and Fabrication

In order to transfer the heat from the asphalt pavement surface to the TEGs, the thermoelectric energy harvesting prototype was developed. This shape of prototype (L-shape) was confirmed with FE analyses, which will be discussed later. The description and schematic of prototype are illustrated in Figure 13.
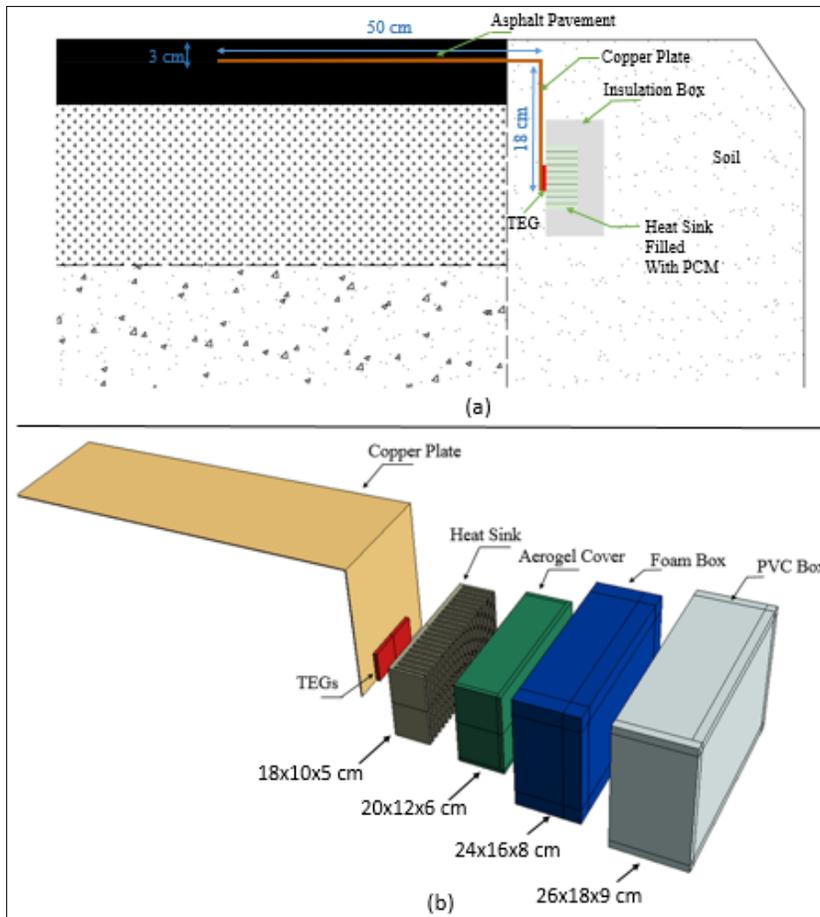
Figure 13. The thermoelectric energy harvesting prototype: (a) schematic of prototype; (b) description of components.

The assembled energy harvesting system consists of four parts:

a. An L-shape copper plate with a thickness of 0.15 cm consisting of two segments: A heat receiver with 50 cm length to collect pavement heat and a vertical heat conductor, with length of 18 cm to convey the heat to the lower pavement layers (Figure 14). The copper plate is well insulated to minimize heat loss. It was shown that the temperature of asphalt pavement 2–3 cm below the surface is about 3–4 °C less than the temperature at the pavement surface (37). Hence, it is desirable to embed the heat collector 2 to 3 cm below the asphalt concrete surface. Furthermore, embedding the heat receiver below the surface of the asphalt concrete layer provides additional protection to this component during routine pavement rehabilitation (e.g., milling and overlaying).
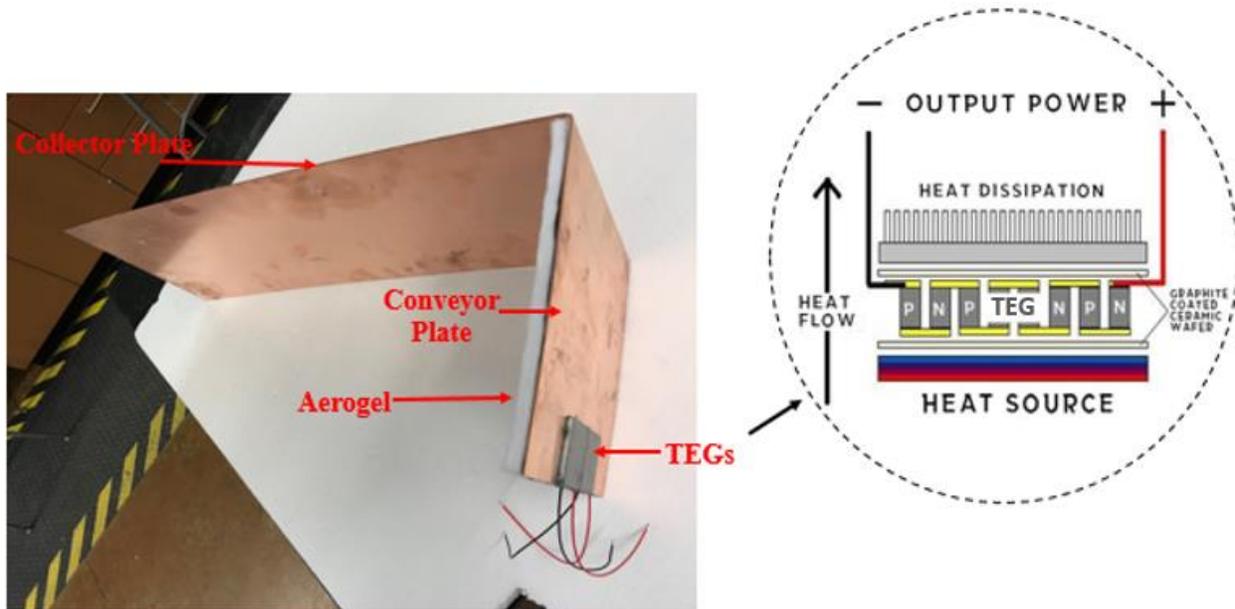
Figure 14. Heat collector plate with Thermoelectric Generator.

b. Two thermoelectric generators to convert thermal energy into electrical energy. The hot sides of the TEGs were attached to the copper plate with thermal paste, while the cold sides were similarly attached to the heat sink. In the presence of a temperature gradient between the two (hot and cold) sides of TEGs, power generation will occur. As shown in Figure 14, each thermoelectric generator consists of a set of alternating P–N elements which are connected in series both electrically and thermally.

c. An aluminum heat sink with a size of $18 \times 10 \times 5$ cm was used for absorbing the heat that inadvertently gets transferred between the hot and cold side of the TEGs (Figure 15-a). Heat sink was filled with a microencapsulated phase change material (MPCM), in a powder form (Figure 15-c), to store the thermal energy by preserving initial temperature (i.e. 18 °C). PCMs are novel materials used in many heat conditioning applications such as heat pump insulation, solar engineering, and spacecraft thermal controls. PCMs have the capability to absorb/release latent heat during their phase transition from solid to liquid and vice-versa (Figure 15-b). Therefore, they are ideally suited for effectively absorbing heat while maintaining the temperature of the heat sink relatively constant (43).
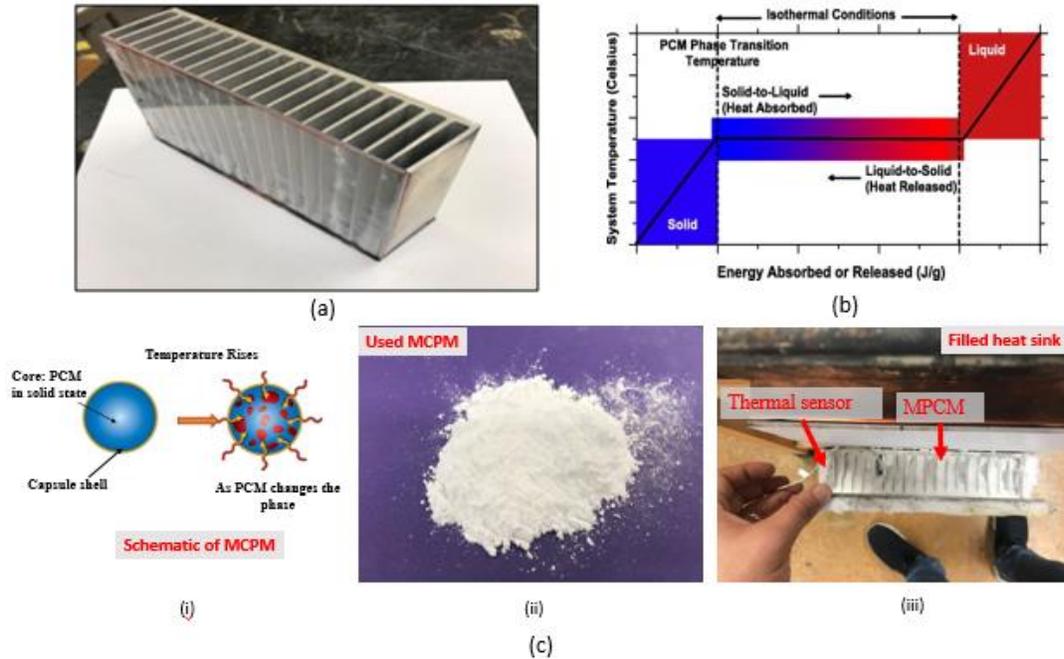
Figure 15. Coolant module: (a) Heat sink; (b) Process of phase changing of PCM (44); (c) Used microencapsulated PCM.

d. The insulation box was designed as a thermal-barrier to prevent the exchange of heat between the heat sink and the surrounding soil (Figure 16). This effectively controls the temperature of the heat sink at the desirable level and maximizes the temperature gradient between the surface and the heat sink, which drives the TEGs. The insulation box consists of three layers: the first layer exposed to ambient temperature, is made of Polyvinylchloride with 1 cm thickness and 0.19 W/(m*K) thermal conductivity; the second layer is expanded Styrofoam with 2 cm thickness and 0.03 W/(m*K) thermal conductivity and the third layer, which is in contact with the heat sink, is Aerogel. Five faces of heat sink were fully covered by Aerogel with thickness of 1 cm and the face having contact with TEGs was partially covered by Aerogel with 0.5 cm thickness. Aerogel, developed by NASA, was used for the Stardust spacecraft as a high insulation barrier due to its low thermal conductivity (i.e., 0.012 W/ m*K) (45, 51). It is currently commercially available at a reasonable price.
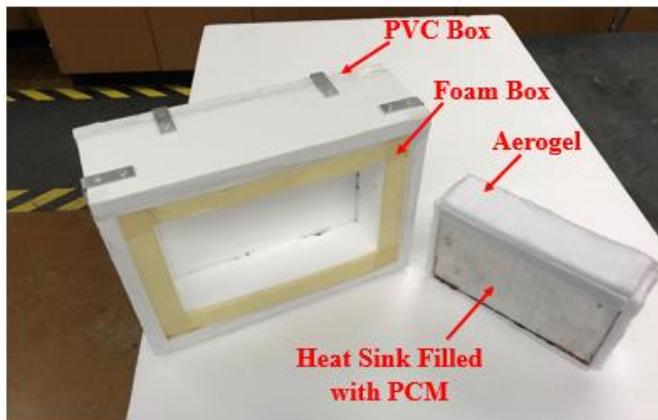
Figure 16. Insulation box

4.5. Finite Element Analysis

Finite element (FE) analysis was conducted using the commercial software ABAQUS to refine the design of the thermoelectric system. A three-dimensional (3D) model of the prototype was constructed for this purpose consisted of the copper plate, TEGs, heat sink and insulation box. Based on FE analyses, the design, length, and width were found as very influential parameters rather than the thickness of plate. Hence, the copper plate with thickness of 0.15 cm, commercially available, was selected. FE analyses provide insights into the thermal behavior of the prototype including thermal gradients, temperature distribution over the time and so on.

This section presents two design models of Z-shape and L-shape plates. The Z-shape model has three parts including a heat collector plate placed into pavement with 50 cm length, a heat conveyor plate with depth of 18 cm and a heat transfer plate with 8 cm length, while the L-shape consists of a heat collector (50 cm) and only a heat conveyor plate (18 cm). The width of the transfer plate was 15 cm for both designs. Note that the idea of Z-shape plate is taken from previous study (36).

The FE analysis was carried out under realistic transient boundary conditions using measured data for the San Antonio area. In this analysis the changes in temperature gradient over time that drives TEG is of interest. As presented in Figure 17, temperature variation at depths of 3, 15, and 20 cm were recorded in the field over five sunny days in San Antonio, TX (Figure 17). This figure indicates the entire range of temperature field corresponding to each depth mentioned above. The higher the temperature, the higher the thermal energy; therefore, the time period throughout the day in which thermal energy can be sufficiently transferred is around 8 hours. Hence, the measured temperature profiles of 8 hours (i.e., 11:00 AM to 7:00 PM) at all three depths were applied on both the Heat collector plate and the insulation box in the FE model.
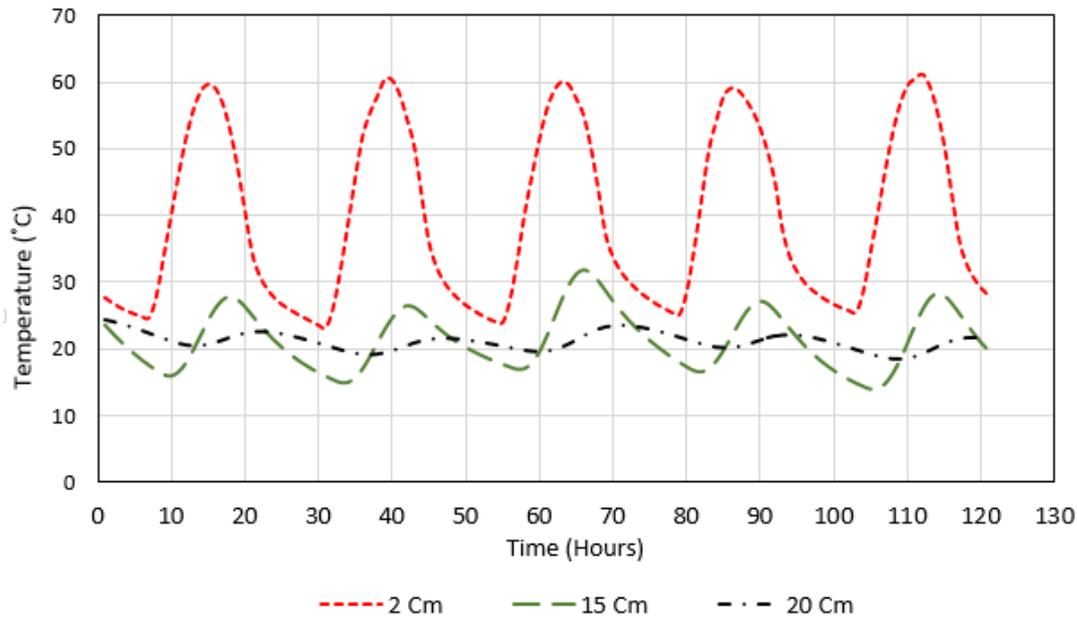
Figure 17. Measured temperature profile (three depths) for five days in San Antonio, TX.

For each material, the properties such as heat conductivity, density and specific heat were defined. The heat flux coming from the pavement surface was utilized as the source of energy on the heat collector plate. Heat flux generally can be obtained using the following equation:

$$q = KA\frac{\Delta T}{\Delta X} \qquad\qquad\qquad\qquad [5]$$

where:

q = the heat flow;

k = the conductivity;

A = the area;

 ΔT = the temperature difference;

Δx = the distance corresponding to this temperature difference.

Figure 18 represents the temperature field results of the Z-shape and L-shape designs during the numerical analysis. As observed in Figure 18 (a and b), top plates in both Z-shape and L-shape models reached the highest temperature of 46 ˚C due to their direct contact with pavement. Moving away from the pavement surface, the temperature decreased to 30 ˚C. Yet, in the provided temperature range (20 to 46 ˚C) the temperature differences between the plates can be barely identified. Thus, Figure 18 (c and d) with a new temperature scale from 33 to 46 ˚C were created to provide a better visual observation for the temperature distributions. Note that all components but the top plate were removed herein.

As depicted, the bottom portion of the Z-shape model roughly reached to 33 ˚C, while at the same region in the L-shape plate reaches 41 ˚C. The significant difference of 8 ˚C can be related to the usage of an extra horizontal component in the Z-shape model attached to the TEGs and resulted in a higher energy loss in the Z-shape model compared to its counterparts. Moreover, FE analyses suggest that in the L-shape model temperature can be transferred much faster down to the TEGs, and consequently a larger thermal energy can be supplied for harvesting purposes.

The temperature distribution of hot side of TEGs connected to plate are presented in Figure 18 (e and f). To provide distinctions between two designs, the temperature range is limited from 20 to 32 ˚C. The insulation boxes enclosing the TEGs in both models reached a similar temperature after 8 hours (i.e., 28 ˚C). However, TEGs in the L-shape model were 2 ˚C higher in magnitude as shown in Figure 18 (e and f). This can be used as an indication that the L-shape plate is more suitable to be employed as a prototype for the purpose of heat transferring. It should be noted that although top plates in the both designs could capture the same amount of heat (Figure 18 (c and d)), the heat dissipation of Z-shape model seemed to be higher.
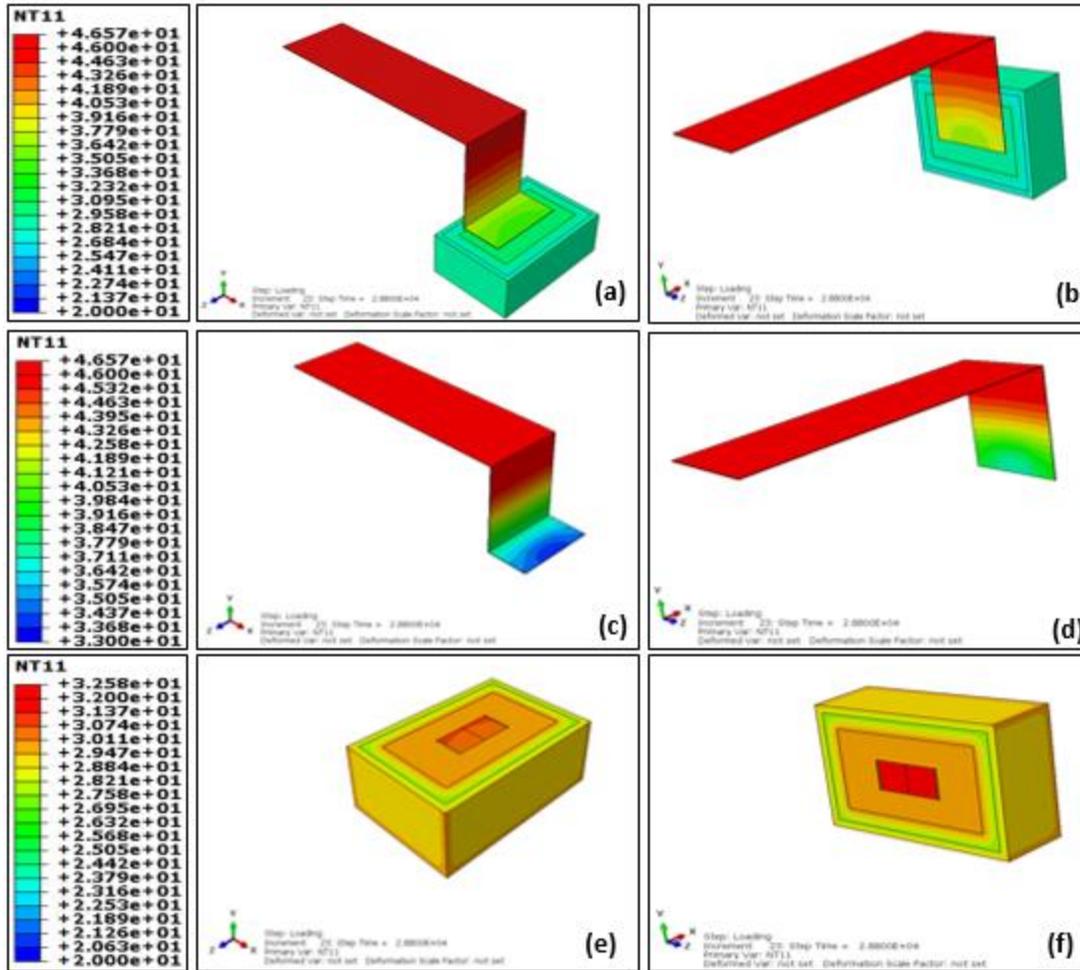
Figure 18. FE analyses of Z-shape and L-shape models.

Since the ultimate intention of using such devices in pavements is to maximize the incoming heat through the surface and increase the amount of energy can be harvested. Therefore, L-shape model is to be considered as an optimum geometry for the rest of this study.

There are several parameters other than geometry that may affect the efficiency of the optimum model. In this section top plate width as one of a key components of heat transfer was investigated. The model with top-plate 15 cm wide along with two different widths of 20 and 25 cm were created (Figure 19). The global behavior of all three models are presented in Figure 19 (a-c). Temperature at the top portion of the L-plate is similar for all three models (average of 47 ˚C), yet the bottom section of the 15 cm plate is almost 4˚C cooler compared to the wider plates. As illustrated in Figure 19 (d-f), due to the larger surface area subjected to the pavement, a higher temperature gradient was generated in 20 and 25 cm plates.
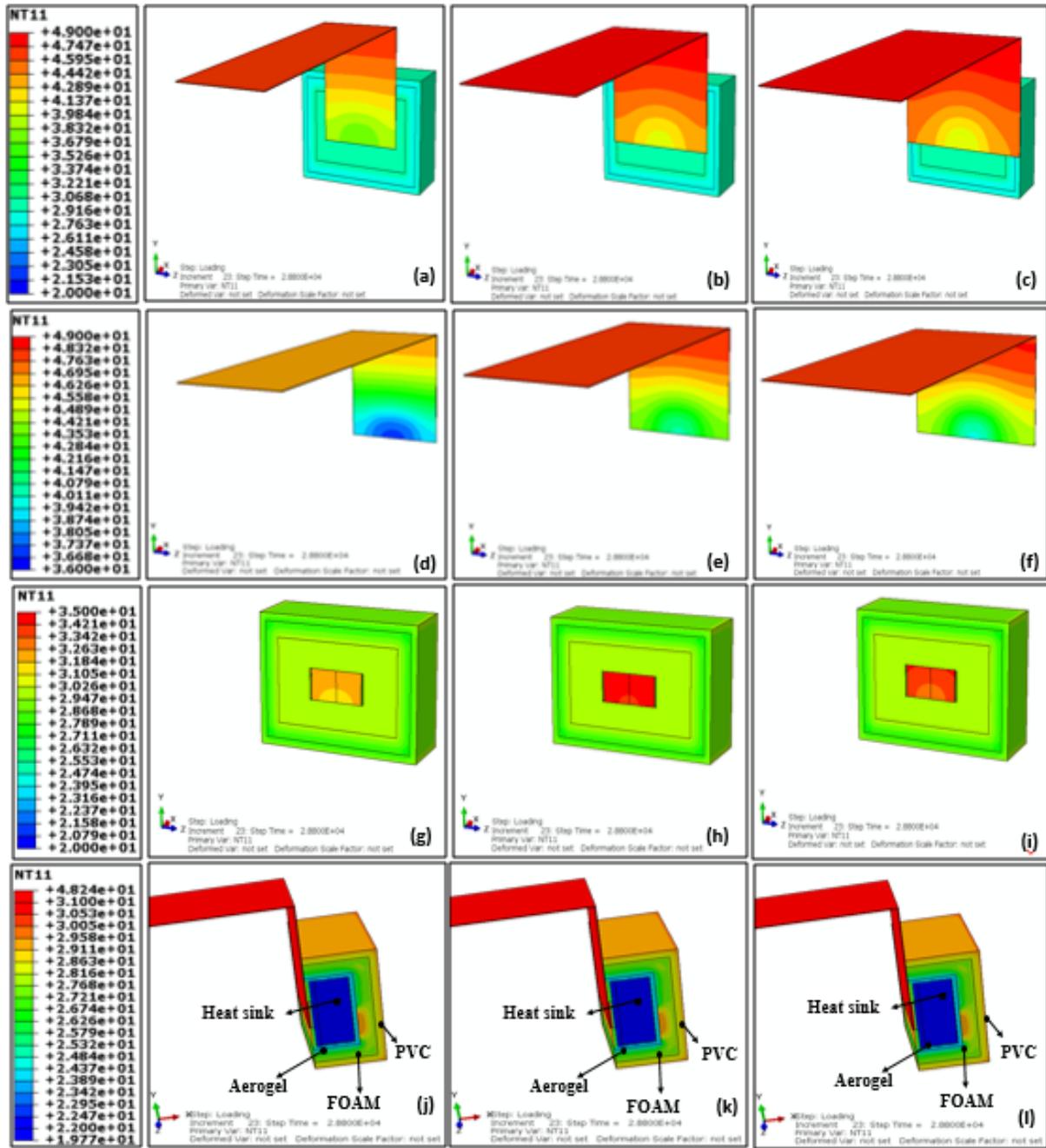
Figure 19. FE analyses results of three different widths models.

In Figure 19 (g-i) top plate parts were removed for the sake of clarity. These figures present the final temperature for TEG and insulation box components after 8 hours of simulation. The significance of these plots is that although increasing the plate width (i.e. 15 cm to 20 and 25 cm) resulted in higher temperature gradients, model with 20 cm plate demonstrated the highest transferred temperature among the three models. As such, the imbedded TEGs in 20 cm model reached to 35 °C during the day, while lower temperature of 34 °C was captured on TEGs 25 cm plate. Thus, considering both the cost efficiency and performance, L-shape plate with a 20 cm

24

width was selected as the optimum model to be tested in field. Table 1 presents the numerical results obtained from plates and TEGs.

Table 1. FE analyses results for determination of optimized design

Designs	High Temp on Collector Plate (˚C)	Low Temp on Conveyor Plate (˚C)	Temp on Hot Side of TEG (˚C)	Temp on Cold Side of TEG (˚C)	Temp Gradient on TEG (˚C)
Z-shaped	46	33	30	19	11
15-L-shaped	46	37	32	19	13
20-L-shaped	48	41	35	19	16
25-L-shaped	48	40	34	19	15

Figure 19 (j to l) are cross sectional views of temperature distributions throughout each component. Based on the analyses, the surface of the outset layer of box (PVC), contacted with the surrounding soil, had the temperature of 30 ˚C; however, the inside of this layer showed 27 ˚C temperature. As it can be seen from the temperature distribution in foam layer, this thermo-barrier could retain more heat energy. The utilization of this layer successfully reduced the temperature of the inner side of the system by 14% (27 to 23 °C). The last layer was Aerogel with low thermal conductivity, which significantly mitigated thermal energy penetration into heat sink. The analyses results indicated that the temperature of heat sink surface was approximately 19 °C, which showed that the insulation box as a thermo-barrier could perform efficiently to reduce penetration of thermal energy from surrounding area. It is worth noting that the FE analyses, conducted in this study, simulated the hottest time period of the day (occurred from 11:00 AM to 7:00 PM) and the proposed insulation box showed proper performance by keeping the heat sink temperature as low as 18-19 °C and improving the overall efficiency of thermal gradient.

4.6. Field Testing, Results and Discussion

Asphalt mix slab (conventional dense graded hot mix asphalt) with thickness of 60 mm were made in the lab and the copper plate was inserted into depth of 30 mm to capture and transfer the pavement heat (Figure 20 (a)). The Heat sink and insulation box were embedded into the bucket filled with soil as presented in Figure 20 (b). The temperature sensors were used to collect the temperature data at four points; surface of asphalt slab, the heat collector plate, inside of the heat sink and the soil at 10 cm depth (Figure 20(c)). The entire porotype was tested in the field between 2:00 pm to 7:00 pm on July 21st (Figure 20 (d)). The TEGs were connected electrically in series into an array to attain larger values of current and voltage. The power meter (Gossen-Metrahit®) was employed to measure the output voltage, current and power.

Figure 20. Field installation and data collection.

The recorded temperatures versus time are plotted in Figure 21. The asphalt surface temperature was varied from 55 to 62 °C. Yet, the associated temperature on the copper plate was recorded between 48 °C and 50 °C. It can be seen that the soil temperature at 10 cm depth increased from 34 to 38 °C. From Figure 21, the lowest and highest temperature magnitudes that the heat sink experienced were 18.3 °C and 18.8 °C, respectively. One of the major accomplishments of this research was to control the temperature of heat sink and maintain the temperature low for the cooling process of the TEGs' cold side. Since the power generation of TEG is considerably affected by thermal gradient, the more temperature difference, the more power can be generated. Therefore, based on the simulations and field test results, the proposed coolant system can properly enhance the efficiency of the thermoelectric asphalt systems by increasing the thermal gradient.
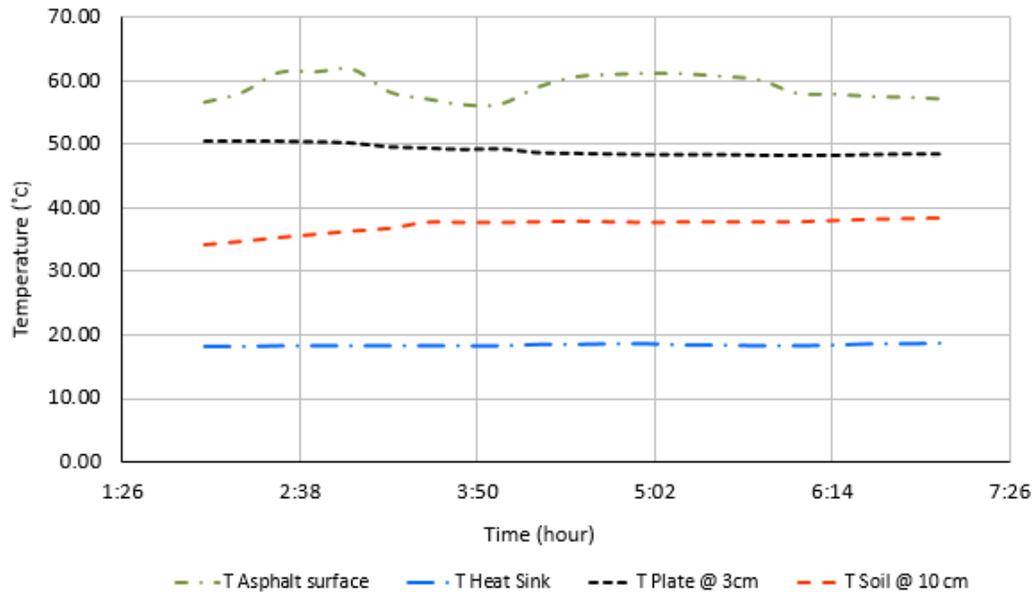
Figure 21. Temperature profile at four depths.

Figure 22 shows the generated power and temperature difference (ΔT) values between the top plate and the heat sink over time traces of 8 hrs. The effect of the diurnal temperature is clearly seen as the power output varies over the time. In this field test, the energy harvester system produced an average power output of 29 mWatt. As illustrated, the maximum power (i.e. 34 mWatt) was captured between 2:00 pm and 2:30 pm when the system exposed to the highest thermal gradient (34 degree); and as temperature decreased, the rate of electric power generation dropped 25 %. As expected, there is a direct correlation between thermal gradient and power output indicating that the higher the thermal gradient, the more the energy available. As mentioned in the literature, our previous study consisted of the Z-shaped plate and two types of coolant module, could generate the maximum power of 14 mWatt, while by incorporating a phase-changing heat sink and L-shaped plate in this study the maximum amount of electricity was raised up to 34 mWatt, demonstrating the significant enhancement of the thermoelectric system generator.
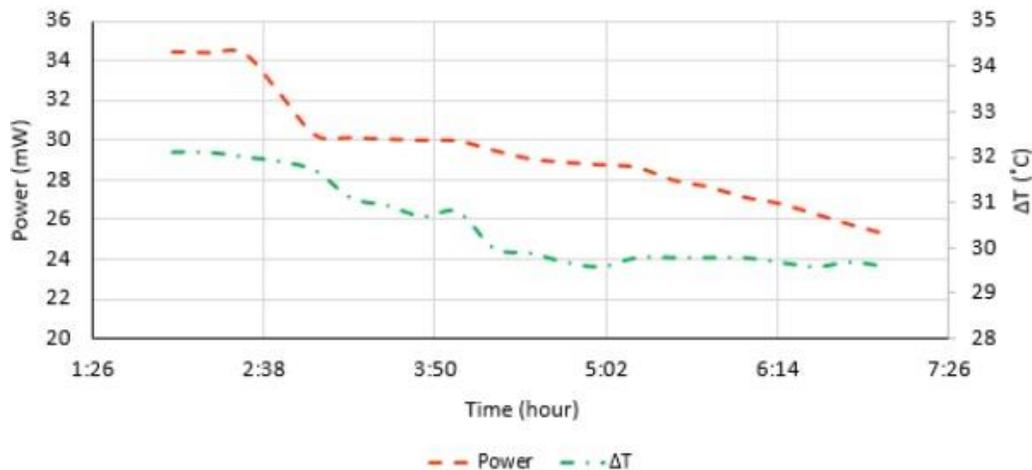
Figure 22. Output power and Temperature Gradient versus Time from Field Tests.

27

5. ANALYSIS AND FINDINGS

This Chapter describes the parametric study and numerical simulation of the prototype model and its lab testing to assess its performance.

5.1. Description of Prototype

Figure 23 depicts the components of the energy harvester system, which mainly consists of four parts including a copper heat collector plate, a TEG device, an aluminum heat sink, and an insulation box. The description of each part is as follows:

1) The heat collector plate is an elongated L-shaped copper plate that has a width of 20 cm and thickness of 0.16 cm. This part has two segments: a) the horizontal segment with length of 50 cm is embedded at 3 cm depth into the pavement surface and gathers the heat from asphalt pavement with thickness of 10 cm, and b) the vertical segment extends up to 20 cm and conveys the heat from the collector down to where it is in contact with TEGs. This segment is also insulated with an aerogel thermal barrier to assist prevention of heat dissipation.

2) In this study, two types of TEGs are used: a) a 4 cm x 4 cm TEG commercially named TXL-199-02Q TEG, and b) a 6.2 cm x 6.2 cm TEG commercially named TXL-287-03Z TEG. Both TEGs are designed for low thermal difference applications. The first type consists of 199 couples (p and n junctions), while the latter one has 287 couples. The hot side of the TEGs is attached to the copper plate, and the cold side is in contact with the heat sink to take advantage of the thermal difference.

3) In order to provide cool temperature for the TEGs, an aluminum heat sink with dimensions of 18 cm x 10 cm x 5 cm was employed. Different materials are usually used in heat sinks to make it more efficient, but in previous studies, the used materials were either soil or water, which could not appropriately keep the temperature down. In this study, microencapsulated phase change material (PCM), in powder form, with an operation temperature of 18°C was used to ensure that the temperature of the heat sink was kept low (Figure 23). PCM with high latent heat storage capacity can absorb a great amount of heat and deliver almost constant temperature. As the temperature rises, the PCM's state changes from solid to liquid, and it continues to absorb thermal energy without a significant increase in temperature. PCMs exhibit the possibility of being used in various applications, such as waste heat recovery, air conditioning in buildings, and spacecraft thermal controls (46).

4) One of the main challenges of the heat sink is to avoid getting warm over time since a heat exchange between the heat sink and the nearby environment (soil or air) is possible, which leads to temperature stabilization. To overcome this issue, a countermeasure is to use the proper insulation to prevent heat exchange. An insulation box with three low thermal conductive materials was developed, which was made of polyvinylchloride, Styrofoam, and aerogel, with thicknesses of 1 cm, 2 cm, and 1 cm, respectively. Aerogels were extensively developed by NASA as a high insulation barrier for its Stardust mission (45).
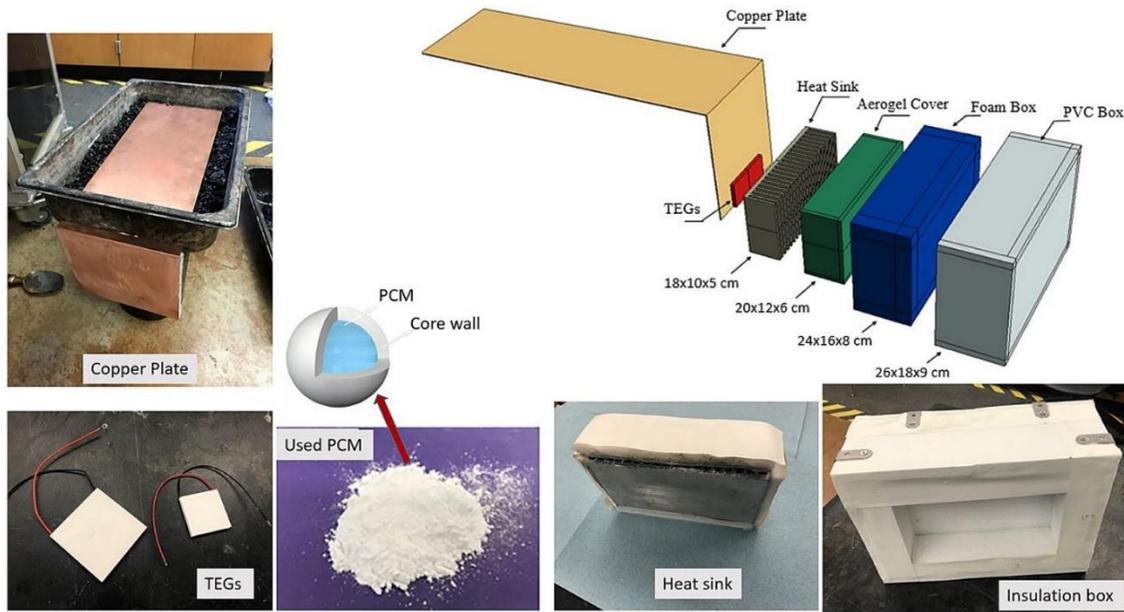
Figure 23. Components of prototype

5.2. Experimental Setup

Figure 24a depicts the side cross-sectional view of the TEG roadway harvester inserted into the road pavement. In order to mimic a real pavement, an asphalt slab with dimensions of 70 cm × 30 cm × 10 cm was fabricated from a dense asphalt mixture (Figure 24b and 24c). The illumination apparatus was an incandescent lamp to simulate solar radiation and apply a realistic temperature to the surface. The height of the lamp can be adjusted to control the intensity of heat over the surface. The top plate of the prototype was inserted 3 cm below the pavement surface to capture heat and transfer it down to the TEGs. The temperature at five spots (the pavement surface, 3 cm below surface, room, bottom of plate, inside of heat sink) were measured by means of two thermometers. To evaluate the effects of temperature on the power output of the system, the TEG was tested within a range of surface temperatures from 45°C to 65°C. Since the number of TEGs and type of TEGs can alter the output power, nine arrangements of TEGs, including five configurations of 4 × 4 cm TEGs and four configurations of 6.2 × 6.2 cm TEGs, were tested at each temperature. The description of each prototype is given in Table 2. The prototypes with four TEGs, in which two TEGs were attached per side to the vertical segment of the plate, employed two coolant modules (Figure 24c).
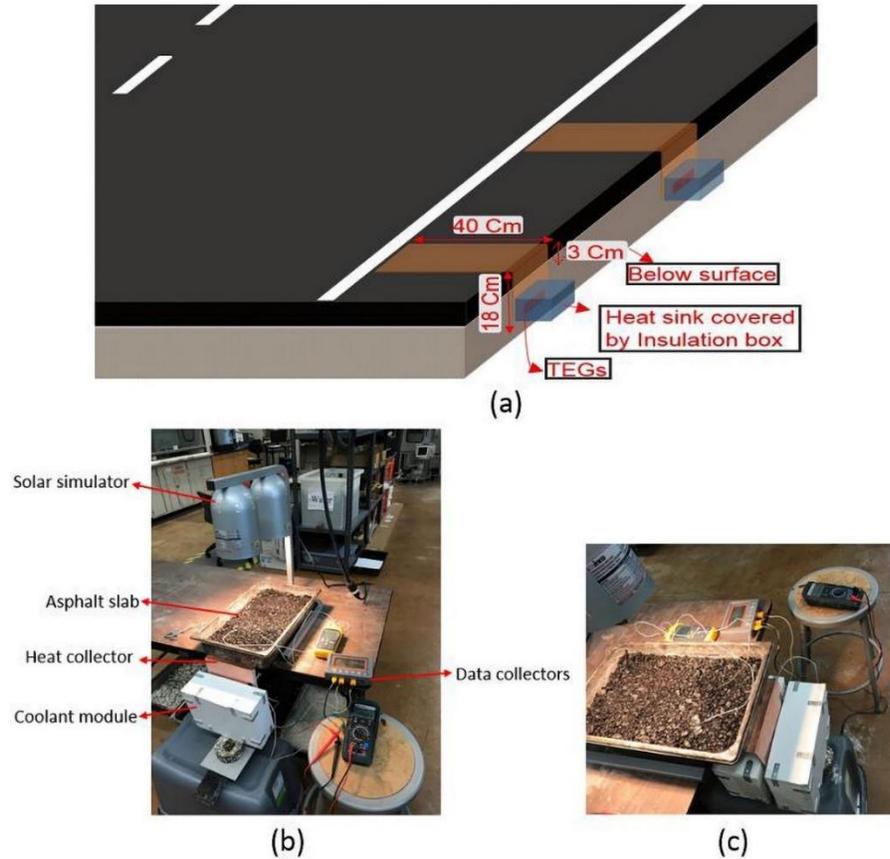
Figure 24. (a) TEG roadway harvester embedded in the road pavement, (b) prototypes with TEGs on one side, (c) prototype with 4 TEGs (2 per side)

Table 2. Details of each tested prototype.

Prototype	Number of TEGs	Size of TEG	Sides of Attachment
1 TEG (4cm-1 side)	1	4×4 cm	1
2 TEG (4cm-1 side)	2	4×4 cm	1
3 TEG (4cm-1 side)	3	4×4 cm	1
4 TEG (4cm-1 side)	4	4×4 cm	1
4 TEG (4cm-2 side)	4	4×4 cm	2
1 TEG (6.2cm-1 side)	1	6.2×6.2 cm	1
2 TEG (6.2cm-1 side)	2	6.2×6.2 cm	1
3 TEG (6.2cm-1 side)	3	6.2×6.2 cm	1
4 TEG (6.2cm-2 side)	4	6.2×6.2 cm	2

5.3. Thermoelectric Theory

Thermoelectric generators are solid-state semiconductor modules that can transform thermal energy directly into electricity based on the Seebeck effect. The Seebeck effect has been widely applied in various thermoelectric-generation technologies (47). Basically, the conductors consist of a uniform distribution of charge carriers, but as they are exposed to a temperature difference, the free carriers at the hot side are prone to spread to the cold side because of their higher kinetic energy. The accumulation of charge leads to a back electromotive force. By maintaining temperature difference across the junctions (parallel n-type and p-type semiconductors), the voltage is generated (47):

$$V = \alpha(T_h - T_c) \tag{6}$$

where:

T_h = the temperature of the hot junctions;

T_h = the temperature of the cold junctions;

α = the difference of the Seebeck coefficient of the p and n semiconductor

The p and n semiconductors within the TEG are connected electrically in series and thermally in parallel. The p and n junctions are inserted between two ceramic plates of high thermal conductivity and low electrical conductivity.

The efficiency of the thermoelectric module can be evaluated by the value of its figure of merit, Z. A higher Z will produce higher conversion efficiency. The figure of merit of thermoelectric efficiency can be expressed as follows (24):

$$Z = \frac{\alpha^2 \sigma}{\lambda} \tag{7}$$

where:

σ and λ = the electrical and thermal conductivity of the material;

The total amount of absorbed heat, Q_H, and heat rejected, Q_C, can be obtained using the standard model proposed by Hodes (30):

$$Q_h = K(T_h - T_c) + (\alpha_p - \alpha_n)IT_h - \frac{RI^2}{2} \tag{8}$$

$$Q_c = K(T_h - T_c) + (\alpha_p - \alpha_n)IT_c + \frac{RI^2}{2} \tag{9}$$

where:

K = the heat transfer coefficient;

I = the current;

R = the internal load resistance;

α_p and α_n = the Seebeck coefficients of the p- and n-type semiconductor

When the TEG device is connected to an external load, the TEG current and power can be obtained as follows (30):

$$I = \frac{V}{R + R_l} \qquad\qquad [10]$$

$$P = Q_h - Q_c = R \times I^2 \qquad\qquad [11]$$

where:

$(Q_h - Q_c)$ = the heat flux due to the temperature gradient;

R_l = the load resistance

5.4. Finite Element Analysis

A finite element analysis via ABAQUS was conducted to investigate how the insulation box could perform as a thermal barrier, how temperature was distributed in the components, and how the number and arrangement of TEGs could impact the efficiency of the harvester system. For input data, the temperature profile of pavement and underground soil was obtained by measuring temperature at three depths (2 cm, 15 cm, and 20 cm) for five days in San Antonio, Texas (Figure 25). To run the analysis, a three-dimensional steady-state heat transfer model was employed, and the boundary conditions applied were the temperatures of 55˚C on the surface of the top plate, 18˚C for the heat sink, and 30˚C for the external surface of the box. Figure 26 presents the different models simulated and analyzed through ABAQUS. For 4 TEGs, two configurations (Figure 26d and e) were developed and analyzed.
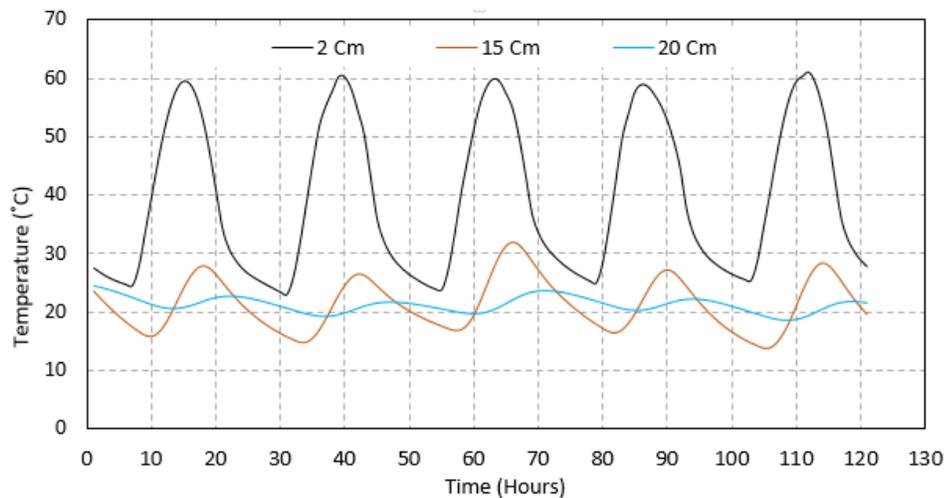
Figure 25. Measured temperatures at three depths over five days.
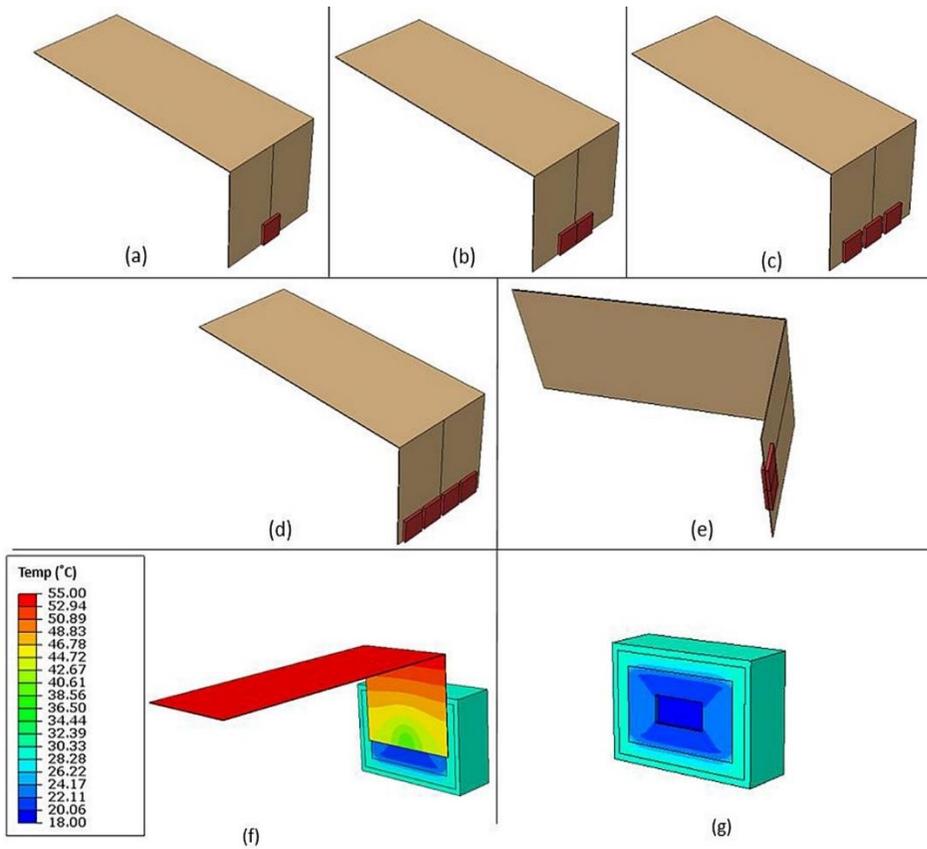
Figure 26. Different FE models: (a) 1 TEG, (b) 2 TEGs, (c) 3 TEGs, (d) 4 TEGs (one side), (e) 4 TEGs (two TEGs per side); (f) thermal distribution of prototype, (g) thermal distribution of coolant system

Figure 26(f) presents how the thermal energy was transferred from the collector plate (horizontal segment) to the conveyor plate (vertical segment). It can be observed that at the top of the conveyor plate, the temperature was around 53°C. Moreover, in the conveyor plate, the amount of heat seemed to diminish as it was conducted from top to bottom; in particular, where the TEG was attached, the temperature decreased as much as 32°C since the TEG absorbed the heat. In Figure 26(g), the temperature distribution throughout the insulation box is illustrated. It is important to note that the temperature dissipation occurred from the outermost layer (PVC) toward the innermost layer (aerogel). The reason is associated with the role of each layer to halt heat penetration from the nearby environment. Here, the environmental temperature of 30°C was considered because actual measurements demonstrated that the soil temperature would not exceed 30°C (Figure 25). The heat dissipation in layers are different due to the differences in thermal properties, especially thermal conductivity. The temperature of the aerogel layer, which was in contact with the heat sink, was around 20-21°C, indicating that the insulation box performed properly as a thermal barrier and preserved the heat sink from getting warm.

The heat transfer model provided insight into the transient temperature distribution within the TEG for each model, which was useful for finding out how the number of TEGs affected the thermal gradient across the TEG. The temperature distribution of TEG surfaces for each model (1 TEG, 2 TEGs, 3 TEGs, and 4 TEGs) is shown in Figure 27. Table 3 presents a summary of the

temperatures driving the thermoelectric harvesting in different models. The simulation results illustrated that the maximum temperatures were 34.89°C, 31.86°C, 29.97°C, 29.12°C, and 30.02°C for Models 1 TEG, 2 TEGs, 3 TEGs, 4 TEGs attached on one side, and 4 TEGs attached on two sides, respectively. Moreover, the minimum temperatures obtained were 18.63°C, 18.75°C, 18.80°C, 20.36°C and 18.65°C for Models 1 TEG, 2 TEGs, 3 TEGs, 4 TEGs attached to one side, and 4 TEGs attached to two sides, respectively. It seems that the minimum temperatures were affected by the quantity and arrangement of TEGs. It can be seen that the minimum temperature of models having up to 3 TEGS were almost similar, while using 4 TEGs (one side) led to an increase of low temperature in the TEGs, which is not desirable for power efficiency. These results indicate that each coolant module might be able to provide low temperature for up to 3 TEG modules, and higher than three modules would exceed the capacity of the coolant module. However, it can be observed that in the model with 4 TEGs attached at two sides, the addition of another coolant module helped keep the temperature of the TEGs low. Additionally, the maximum temperatures on the hot side of the TEGs are different for all simulations. For the model with 1 TEG, the maximum temperature on the hot side is 3.03°C larger than the one with 2 TEGs and is approximately 5°C larger than the other models. This finding demonstrated that the increase in the number of TEGs reduced the amount of heat absorbed by each TEG, which would lower the temperature difference across the TEG. From the results, although the model with one TEG achieved a greater temperature difference than the others, other arrangements provided a higher capacity for the prototype. In other words, it might be expected that using a higher number of TEGs would increase the amount of power. However, the data in Table 3 indicate that the model with 4 TEGs on one side exhibited the lowest thermal gradient, which therefore is not the optimal design for the prototype. Nonetheless, the experimental results revealed the amount of actual power generated by each model, allowing a comparison between models in terms of power generation and economics.

Table 3 Summary of temperature gradient for each model.

Model	Temp. at Hot Side (°C)	Temp. at Cold Side (°C)	Effective Temp. Gradient (°C)
1 TEG	34.89	18.63	16.26
2 TEG	31.86	18.75	13.11
3 TEG	29.97	18.80	11.17
4 TEG (1 side)	29.12	20.36	8.76
4 TEG (2 side)	30.02	18.65	11.37
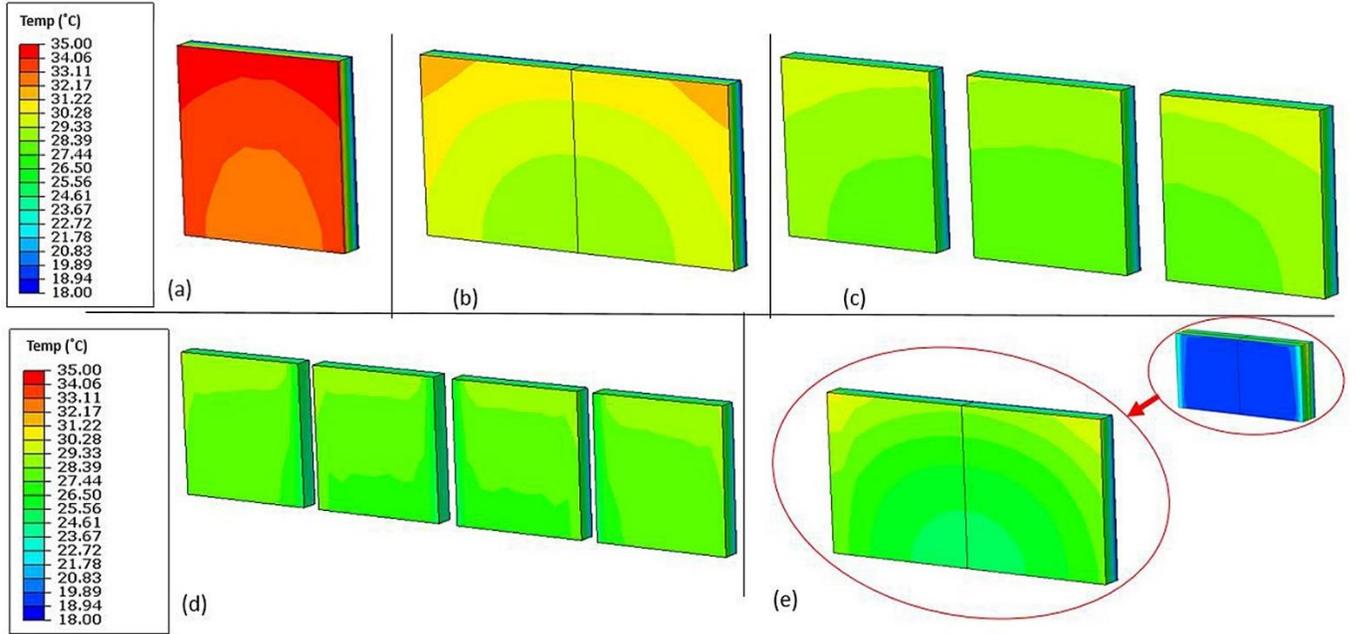
Figure 27. Different FE simulations: (a) 1 TEG model, (b) 2 TEG model, (c) 3 TEG model, (d) 4 TEG in one side model. (e) 4 TEG (two per side) model.

5.5. Laboratory Test Results

Figures 28a-c show the power generated from the energy harvesting prototypes over 5 hr at temperature of 45, 55, and 65°C respectively. Moreover, the temperature profile for the asphalt slab surface, the depth of 3 cm, the bottom of the copper plate, and the heat sink corresponding to each temperature (45, 55, 65°C) is presented in Figures 28d-f. Table 4 presents the summary of power output produced by different prototypes. As shown in Figure 28a, the 4 TEG (6.2-2 side) prototype produced 47.14 mWatt, which was the highest amount of power, and the lowest power output was obtained by 1 TEG (4-1 side) prototype with a magnitude of 18.9 mWatt. In addition, a reductive trend of power can be seen as the number of TEGs increases. For example, the addition of one TEG module to the 1 TEG (4-1 side) prototype increased power by 57.4% to 29.74 mWatt, while the increase rate of the 3 TEG (4-1 side) prototype relative to the 2 TEG (4-1 side) was 23.5%.

The possible reason for such results is that increasing the number of TEGs could negatively affect ΔT for each TEG, which is a key factor for power generation. Every single TEG would absorb a certain amount of heat from copper plate, and the addition of more TEGs could make each TEG absorb less heat relative to its previous state (fewer numbers of TEGs). Also, the addition of a TEG imposes more heat to the heat sink; therefore, the heat sink might not provide a temperature as cold as before. As a result, each TEG would experience less ΔT, thus impacting the power production of the system. The effect of the number of TEGs on the heat sink and consequent power can be observed when four TEGs are used. The 4 TEG (4-1 side) prototype, employing one heat sink for four TEGs, showed 8.8% larger power than the 2 TEG (4-1 side); however, the 4 TEG (4-2 side) prototype, taking advantage of two heat sinks (one for each pair of TEGs), revealed 19.43% greater power relative to the 2 TEG (4-2 side). This indicates that the application of four 4×4 cm TEG modules may exceed the cooling capacity of the heat sink. The obtained results are in

agreement with what derived from FE simulations, which suggested that using four TEGs on one side would establish the lowest thermal gradient.

In the case of using the 6.2×6.2 cm TEG, the 1 TEG (6.2-1 side) produced 23.5 mWatt power, which was 24.33% larger than the 1 TEG (4-1 side). An interesting point was observed during simulations—the similar power generated by the 3 TEG (4-1 side) and the 3 TEG (6.2-1 side), which was 36.74 and 35.03 mWatt, respectively. This result might be due to the same reasons previously discussed that using three 6.2×6.2 cm TEGs might surpass the capacity of heat sink, and although the number of TEGs was increased, it could not outperform the effect of reduced ΔT. Furthermore, the 4 TEG (6.2-2 side), with the help of two heat sinks, produced the power of 47.14 mWatt, which is 31 % higher than the 2 TEG (6.2-1 side) prototype.

Figure 28b represents a similar trend that can be observed in power output when the prototypes were examined under 55˚C. With the temperature profile shown in Figure 28e, the temperature at the asphalt surface, a depth of 3 cm, the bottom of the plate, and the inside of the heat sink reached 55.3, 46.8, 34.26 and 18.1˚C, respectively. For the output power, Figure 28b shows that the power produced from the energy harvesters increased and then trended to constant when the temperature of the asphalt slab attained constant value. The maximum power achieved by the 4 TEG (6.2-2 side) prototype was 36.16 mWatt. In addition, no substantial difference was found between the performances of the 4 TEG (6.2-2 side) and 4 TEG (4-2 side) prototypes. As the temperature reduced from 65˚C to 55˚C, the power output differences became less. The 1 TEG (4-1 side) prototype revealed the lowest power (16.77 mWatt), which increased by 48.8% up to 24.95 mWatt when the 1 TEG module was added (2 TEG [4-1 side]). Additionally, the 1 TEG (6.2-1 side) prototype produced power of 19.14 mWatt, which rose by 47 % up to 28.7 mWatt by the addition of another TEG (2 TEG [6.2-1side]); however, it must be noted that the addition of another TEG (3 TEG [6.2-1 side]) did not make any difference in power output relative to the 2 TEG (6.2-1side), and these prototypes exhibited almost the same power.
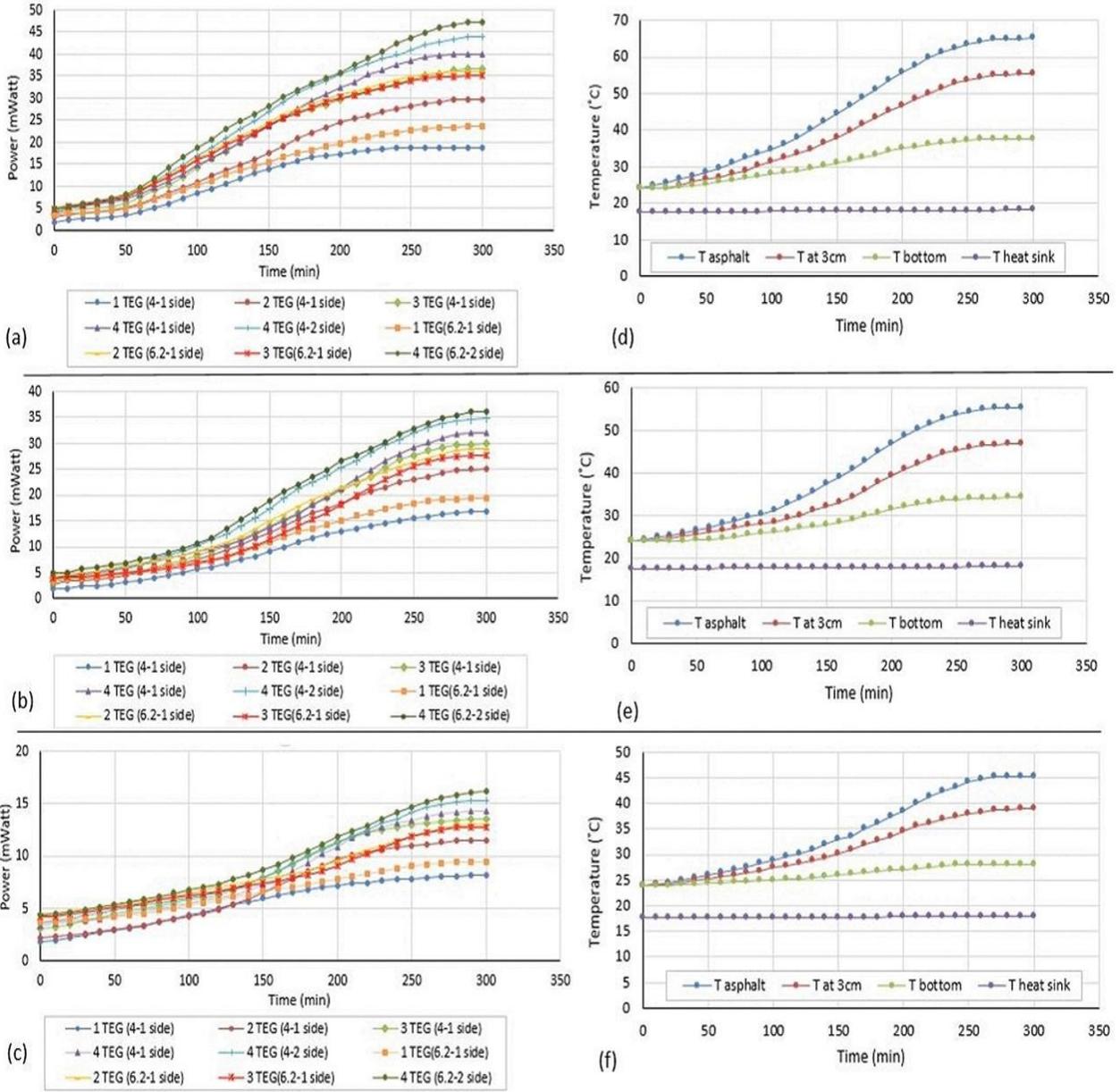
Figure 28. (a) Electrical output from different TEG energy harvesters under (a) 65˚C, (b) 55˚C, 45˚C; temperature profile at different spots under (d) 65˚C, (e) 55˚C, (f) 45˚C

Table 4 The summary of power outputs generated by different prototypes

Prototype	Power (mWatt) at 45℃	Power (mWatt) at 55℃	Power (mWatt) at 65℃
1 TEG (4cm-1 side)	8.14	16.77	18.9
2 TEG (4cm-1 side)	11.51	24.95	29.74
3 TEG (4cm-1 side)	13.05	29.85	36.74
4 TEG (4cm-1 side)	14.32	32.08	32.35
4 TEG (4cm-2 side)	15.34	35.07	35.51
1 TEG (6.2cm-1 side)	9.45	19.14	23.5
2 TEG (6.2cm-1 side)	12.6	28.7	35.98
3 TEG (6.2cm-1 side)	12.49	27.96	35.03
4 TEG (6.2cm-2 side)	16.18	36.16	47.14

Figure 28f shows that the temperature at the asphalt slab surface rose to 45°C over 5 h and also shows that the temperature at the 3 cm depth, the bottom of the plate, and inside of the heat sink were 38.96, 28.09 and 18.01°C, respectively. The power output of different prototypes corresponding to the temperature (e.g., 45°C) is presented in Figure 28c. It can be seen in Figure 28c that the power level of prototypes decreased as the temperature of the asphalt slab reduced to 45°C. Under this condition, the 4 TEG (6.2-2 side) prototype revealed a maximum power of 16.18 mWatt, and as expected, the lowest power obtained was 8.14 mWatt by the 1 TEG (4-1 side). In addition, the 2 TEG (4-1 side) could generate power of 11.51 mWatt, which is 41.5 % greater than the 1 TEG (4-1 side). The 4 TEG (4-1 side) generated power of 14.32 mWatt, which is slightly higher than the 3 TEG (4-1 side) prototype (e.g. 6 %). The 4 TEG (4-2 side) prototype performed properly and produced 15.34 mWatt, which is the highest value among the prototypes employing the 4×4 cm type module. In the case of the 6.2×6.2 cm module, the 1 TEG (6.2-1 side) showed a power of 9.45 mWatt, which was increased by 33% up to 12.6 mWatt by 2 TEG (6.2-1 side), but the addition of another TEG did not increase the power (3 TEG [6.2-1 side]).

Since the power output of the TEG module is dependent on the temperature differential, the performance of the coolant module can impact the efficiency of the energy harvester prototype. Although the room temperature was around 23-24°C (Figures 27d-f), the temperature of the heat sink was kept around 18°C with the help of the coolant system developed for this study. This result indicates that on one hand the aluminum heat sink filled with PCM could perform well and provide temperature as low as 18°C and, on the other hand, the three-layer insulation box is capable of preventing heat exchange between the heat sink and the surrounding environment. Thus, compared to efforts in previous studies, this proposed coolant system can be a more efficient method to supply low temperatures for TEG modules.

From the results, it can be concluded that the 2 TEG (4-1 side), 2 TEG (6.2-1 side), 4 TEG (4-2 side) and 4 TEG (6.2-2 side) prototypes could perform efficiently in terms of ratio of power to number of TEGs. Moreover, it can be inferred that the coolant module would be appropriate for employing up to three 4×4 cm TEGs and/or two 6.2×6.2 cm TEGs. If a higher number of TEGs are intended to be employed for greater power production without efficiency loss, using a bigger heat sink that will allow the use of a higher amount of PCM or using a heat sink exclusively for a

certain number of TEGs based on the type of module (e.g., 4×4 cm or 6.2×6.2 cm) is recommended.

Thermal harvesting prototypes show great potential for the production of clean power that can be used to supply energy for low-power roadside applications, such as wireless sensors, structural health monitoring (SHM), communication systems, and LED traffic lights. For instance, Karsilayan et al have recently developed the SHM system, consisting of a DC-DC booster, a buck controller, a microcontroller and a wireless sensor for transmitting the data. The total power required to activate the system is 3.18 mWatt and the proposed system is capable of monitoring bridge and pavement condition by collecting data on critical response parameters. Accordingly, the 2 TEG (4-1 side) prototype can power approximately 10 of such SHM devices without the need for external grid power. Regarding the demand for utilizing such systems in roads, the appropriate thermoelectric harvesting system can be employed based on the required power for roadside systems (53).

6. CONCLUSION

This section aims to estimate the capacity of the proposed energy harvester installed in roadways. Experimental results suggested that the prototype with area of 0.5 m x 0.2 m (top plate) would generate an average power output (P_{ave}) of 29 mWatt or 835 J over 8 hours per day. Therefore, the power output of pavement per square meter (P_{Sm}) can be expressed as follows:

$$P_{Sm} = (P_{ave})/A_t = (29)/(0.2 \times 0.5) = 290 \ mWatt/m^2 \qquad [1]$$

where:

A_t = the area of top plate.

To elaborate about the scale of power production, in the instance of a pavement road with 10 m width and 1 km length accompanied by an embedded copper plate of 0.5 m × 0.2 m, an average power production of pavement section (P_{Ps}) can be calculated using the following equation:

$$P_{Ps} = P_{Sm} \times A_{Ps} = 290 \times (1000 \times 10) = 2900 \ Watt \qquad [2]$$

where:

A_{Ps} = pavement section area.

Accordingly, the generated power by this pavement section over 8 hours (P_{8h}) can be obtained as follows:

$$P_{8h} = P_{Ps} \times Hours = 2900 \times 8 = 23.2 \ kWh \qquad [3]$$

Or,

$$P_{8h} = P_{ps} \times Seconds = 2900 \times 8 \times 3600 = 83.5 \times 10^6 J \qquad [4]$$

Based on the calculations, the output energy will be as high as 83.5×10^6J over 8 h, equivalent to 23.2 kWh of electricity. It is reasonable to conclude that more power generation can be obtained in warmer regions where roadways are exposed to the direct sunlight for a longer period of time.

In order to evaluate the efficacy of the proposed system, the list of the current road energy harvester technologies is presented in Table 5 (50).

Table 5. Energy generation of current road energy harvester technologies.

Technology	Company/researcher	Maximum power density
Photovoltaic	Solar Roadways	Not analyzed
Piezoelectric	Yesner et al.	1.03 mW/cm^3
	Zhao et al.	0.75 mW/ cm^3
TEG	Datta et al.	1.457 mW/cm^3
	Wu and Yu	2.6 mW/cm^3
	Jiang et al.	2.83 mW/cm^3

Dividing the maximum power (34 mWatt) over the dimensions of two TEGs (2 x 4 cm x 4 cm x 0.35 cm) would provide the maximum power density about 3.02 mW/cm3 which is higher compared with the previous thermoelectric energy harvesters. Such an environmentally friendly electricity can be potentially stored and used as a self-powered source of low-watt electrical facilities such as wireless monitoring systems and pavement health monitoring in remote areas in where electric grid power is not available.

6.1. Economic Analysis

The Levelized Cost of Energy (LCOE) is a method to assess the cost of energy production of a given system. The LCOE is a decisive parameter in power industry and can be used to compare the unit cost of the output power generated from nonrenewable energy sources (i.e., fossil fuels) and well-developed renewable sources, like photovoltaics. This parameter is defined as the ratio of the annualized capital expenditure for construction/operation/maintenance (O&M) divided by the annual energy output ($/kWh) (1)

$$LCOE = \frac{Annualized\ Capital\ Expenditure + O\&M}{Annual\ System\ Output} \qquad [5]$$

The capital expenditure for the prototype system was found approximately $150 considering both construction and installation. Note that the cost of operation and maintenance were assumed to be negligible. With assumption of service life of 20 years and a discount rate of 3%, the annualized cost of $7.5 per unit was yielded. The LCOE of the proposed thermoelectric energy harvester for road pavement with 10 m width was achieved as 0.9 $/kWh per meter based on the average output power for 8 h.

The unit cost of the electricity produced from fossil fuels is determined by the sum of the unit sale price charged from the electrical plant plus the social cost of carbon dioxide emissions (SC-CO2). In 2015, the unit sale price for network power was in the range of $0.065kWh to $0.123kWh. Based on the Environmental Protection Agency (EPA) estimates, SC-CO2 is the main contributor of climate change damages causing changes in human health; net agricultural productivity; property damages from increased flood risk; and changes in energy system costs such as reduction of costs for heating and increase of costs for air conditioning (48).

The average value of SC-CO2 was estimated at $56 per metric ton of CO2 emissions in 2007. Adjusted for inflation in 2016, it would be $64 per metric ton of CO2 emissions (35). Depending on the type of fuel used to produce the power, the amount of CO2 in terms of kWh of electricity varies. This value for gas and coal was ranged from $0.035kWh to $0.062kWh, respectively. The summation of these two costs, power plant and SC-CO2, yields a cost estimation of $0.20kWh.

According to the current laboratory development and the power generation capacity of the thermoelectric generator, this technology might not be economically competitive with electric grid, but environmentally it can generate no emissions of greenhouse gases and particulate matters during operation leading to a low-carbon future and reduction of urban heat island. Nevertheless, the application of the developed system is to build a self-contained continuous electricity generator for installation anywhere in the roadway network far away from power supply facilities. The generated electricity can be stored and supply power for electric vehicles, sensors network, traffic data acquisition systems, and enhance safety through illumination of LED traffic lights and warning signs and deicing/defrosting roadway surface.

REFERENCES

1. Roshani H, Jagtap P, Dessouky S, Montoya A, Papagiannakis AT. Theoretical and experimental evaluation of two roadway piezoelectric-based energy harvesting prototypes. *Journal of Materials in Civil Engineering*. 2017 Nov 17;30(2):04017264.

2. Purohit, I., Purohit, P., and Shekhar, S.. Evaluating the potential of concentrating solar power generation in Northwestern India. *Energy policy*, 2013 62, 157-175.

3. Khan, J., and Arsalan, M. H.. Solar power technologies for sustainable electricity generation–A review. *Renewable and Sustainable Energy Reviews*, 2016. 55, 414-425.

4. Dezfooli, A. S., Nejad, F. M., Zakeri, H., & Kazemifard, S. Solar pavement: A new emerging technology. *Solar Energy*, 2017. 149, 272-284

5. Gholikhani, M., Roshani, H., Dessouky, S., and Papagiannakis, A. T. A critical review of roadway energy harvesting technologies. *Applied Energy*, 2020. 261, 114388.

6. Ahmad, S., Abdul Mujeebu, M., and Farooqi, M. A. Energy harvesting from pavements and roadways: A comprehensive review of technologies, materials, and challenges. *International Journal of Energy Research*.2019

7. Walubita LF, Sohoulande Djebou DC, Faruk AN, Lee SI, Dessouky S, Hu X. Prospective of Societal and Environmental Benefits of Piezoelectric Technology in Road Energy Harvesting. *Sustainability*. 2018 Feb 1; 10(2):383.

8. Wang, H., Jasim, A., and Chen, X. Energy harvesting technologies in roadway and bridge for different applications–A comprehensive review. *Applied Energy*, 2018. 212, 1083-1094.

9. Sodano, H.A., Inman, D.J., and Park, G. A Review of power harvesting from vibration using piezoelectric materials. *The Shock and Vibration Digest*, 2004. Vol. 36, No. 3, pp. 197 – 205.

10. Morbiato, T., Borri, C., and Vitaliani, R. Wind energy harvesting from transport systems: A resourse estimation assessment. *Journal of Applied Energy*, 2014. Vol 133, pp. 152-168

11. Bhattacharjee, S., Batra, A. K., and Cain, J. Energy harvesting from pavements using single crystal and nano-composite smart materials, T & DI Congress, 2011.

12. HybridCARS, http://hybridcars.com Accessed Aug 14, 2016.

13. Voigt, T., Ritter, H. and Schiller, J. (2003). Utilizing Solar Power in Wireless Sensor Networks. Proceedings of the 28th Annual IEEE International Conference on Local Computer Networks, No. 20-24, pp:416-422.

14. De Bondt, A. (2003). Generation of Energy via Asphalt Pavement Surfaces. Asphaltica Padova.

15. Liu, X., Rees, J. S. and Spitler, D. J. (2007). Modeling snow melting on heated pavement surfaces. Part I: Model development. Journal of Applied Thermal Engineering, Vol 27, pp:1115 –1124

16. Dawson R.A., Dehdezi, P.K., Hall, R.M., Wang, J. and Isola, R., 2011. "Thermo-Physical Optimization of Asphalt Paving Materials", Transportation Research Board (TRB), Annual Meeting, Washington, USA, January 2012.

17. Gao Q, Huang Y, Li M, Liu Y, Yan Y. Experimental study of slab solar collection on the hydronic system of road. Solar energy. 2010;84(12):2096-102.

18. Nordmann, T., Froelich, A., Goetzberger, A., Kleiss, G, et al., "The Potential of PV Noise Barrier Technology in Europe", Proceedings at the 16th European Photovoltaic Solar Energy Conference and Exhibition, Glasgow, United Kingdom, May 2000

19. Nordmann, T. and Clavadetscher, L., 2004. "PV on Noise Barriers", Journal of Progress in Photovoltaics: Research and Applications, 12: 485–495

20. Grasselli, U., Schirone, L. and Bellucci, P. "Infrastructures Integration of Photovoltaic Power", Proceedings of the International Conference on Clean Electrical Power (ICCEP '07), May 2007, Capri, Italy

21. Symeoni, A., 2012, "A review on energy harvesting from roads", MSc Environmental Engineering & Sustainable Infrastructure, [TSC-MT 12-017], KTH Royal Institute of Technology.

22. SolaRoad. http://en.solaroad.nl/publications/   Accessed June 24, 2016.

23. Kang-Won, W. and Correia, A., J., 2010. "A Pilot Study for Investigation of Novel Methods to Harvest Solar Energy from Asphalt Pavements". Korea Institute of Construction Technology (KICT).

24. Selvaraju, R.K., "Characterization of Solar Roadways via Computational and Experimental Investigations" (2012). University Of Western Ontario - Electronic Thesis and Dissertation Repository. Paper 906.

25. Golden, J., S., Carlson, Kaloush, E., K, and Phelan, P., 2007. "A comparative study of the thermal and radiative impacts of photovoltaic canopies on pavement surface temperatures", Journal of Solar energy, 81: 872–883

26. Strauss, D., Fehr, R., and Cain, A., 2009. "Vehicle Surfaces: A Parking Lot PV Solar Energy Power Generation System", SAE International.

27. Mallick, R.B., Chen, B. L. and Bhowmick, C. "Harvesting energy from asphalt pavements and reducing the heat island effect", *International Journal of Sustainable Engineering*, 2009. 2:3, 214-228

28. Mallick RB, Chen BL, Bhowmick S. Harvesting heat energy from asphalt pavements: development of and comparison between numerical models and experiment. *International Journal of Sustainable Engineering*. *2012* 1;5(2), pp. 159-69.

29. Wu, G., & Yu, X. Thermal energy harvesting across pavement structure. *Proceedings of the Transportation Research Board (TRB) 91st Annual Meeting* (No. 12-4492). 2011.

30. Wu, G., and Yu, X. System design to harvest thermal energy across pavement structure. *IEEE Energy Tech. 2012* (pp. 1-4). Cleveland, OH

31. Hill, D., Agarwal, A., and Tong, N. Assessment of piezoelectric materials for roadway energy harvesting. *Energy Research and Development Division Final Project Report, DNV KEMA Energy & Sustainability*, Oakland, CA, 201414. Ali, S. F., Friswell, M. I., and Adhikari, S., Analysis of energy harvesters for highway bridges. *Journal of Intelligent Material Systems and Structures*, 2011. Vol. 22, No. 16, , pp. 1929-1938

32. Xiong, H., Piezoelectric energy harvesting for public roadways, Ph.D. Dissertation, *Virginia Polytechnic Institute and State University, Department of Civil Engineering*, VA, 2014.

33. G. Liang, P. Li.Research on thermoelectrics transducers for harvesting energy from asphalt pavement based on seebeck effects. *Advances in civil engineering and building materials*.2015 CRC Press, p. 339

34. Ahiska R, Dişlitaş S. Computer controlled test system for measuring the parameters of the real thermoelectric module. *Energy conversion and management*. 2011 Jan 1;52(1), pp. 27-36.

35. Hasebe, M., Kamikawa, Y., and Meiarashi, S.. Thermoelectric generators using solar thermal energy in heated road pavement. *25th International Conference on Thermoelectrics*. 2006 (pp. 697-700). IEEE. Vienna.

36. Datta U, Dessouky S, Papagiannakis AT. Harvesting thermoelectric energy from asphalt pavements. *Transportation Research Record: Journal of the Transportation Research Board*. 2017 Aug 1(2628), pp. 12-22.

37. Jiang W, Yuan D, Xu S, Hu H, Xiao J, Sha A, Huang Y. Energy harvesting from asphalt pavement using thermoelectric technology. *Applied Energy*. 2017 Nov 1; 205, pp. 941-50.

38. Wu, G., & Yu, X. B. . Computer-aided design of thermal energy harvesting system across pavement structure. *International Journal of Pavement Research and Technology*, 2013 6(2), 73-79.

39. Jiang W, Xiao J, Yuan D, Lu H, Xu S, Huang Y. Design and experiment of thermoelectric asphalt pavements with power-generation and temperature-reduction functions. *Energy and Buildings*. 2018 Jun 15; 169, pp. 39-47.

40. Duarte F, Ferreira A. Energy harvesting on road pavements: state of the art. *Proceedings of the institution of civil engineers*. 2016 Mar 8; 169, pp. 79-90.

41. Lau, P. G., & Buist, R. J. (). Calculation of thermoelectric power generation performance using finite element analysis. *In XVI ICT'97. Proceedings ICT'97. 16th International Conference on Thermoelectrics*. 1997 (Cat. No. 97TH8291) (pp. 563-566). IEEE.

42. Liu C, Chen P, Li K. A 1 KW thermoelectric generator for low-temperature geothermal resources. InProceedings, *Thirty-Ninth Workshop on Geothermal Reservoir Engineering*, 2014 Feb 24 Stanford University, Stanford, California.

43. Sharma A, Tyagi VV, Chen CR, Buddhi D. Review on thermal energy storage with phase change materials and applications. *Renewable and Sustainable energy reviews*. 2009 Feb 1; 13(2):318-45.

44. Fernandes F, Manari S, Aguayo M, Santos K, Oey T, Wei Z, Falzone G, Neithalath N, Sant G. On the feasibility of using phase change materials (PCMs) to mitigate thermal cracking 45. Jelle BP, Hynd A, Gustavsen A, Arasteh D, Goudey H, Hart R. Fenestration of today and tomorrow: A state-of-the-art review and future research opportunities. *Solar Energy Materials and Solar Cells*. 2012 Jan 1; 96, pp. 1-28.

46. Jaworski, M., Bednarczyk, M., & Czachor, M. Experimental investigation of thermoelectric generator (TEG) with PCM module. *Applied Thermal Engineering*, 2016. 96, 527-533.

47. Merienne, R., Lynn, J., McSweeney, E., & O'Shaughnessy, S. M. Thermal cycling of thermoelectric generators: The effect of heating rate. *Applied Energy*, 2019. 237, 671-681.

48. Ewart LM, McLaughlin EA, Gittings KD. Investigation of the compressive material properties of PZT and PMN. *Naval undersea warfare center newport div ri*; 1999 Dec 1. https://apps.dtic.mil/dtic/tr/fulltext/u2/a379761.pdf

49. LeBlanc S. Thermoelectric generators: Linking material properties and systems engineering for waste heat recovery applications. *Sustainable Materials and Technologies*. 2014 Dec 1; 1, pp. 26-35.

50. Sun W, Lu G, Ye C, Chen S, Hou Y, Wang D, Wang L, Oeser M. The State of the Art: Application of Green Technology in Sustainable Pavement. *Advances in Materials Science and Engineering*. 2018.

51. Whalen SA, Dykhuizen RC. Thermoelectric energy harvesting from diurnal heat flow in the upper soil layer. *Energy conversion and management*. 2012 Dec 1; 64, pp.397-402.

52. Wang Z, Zhang S, Yao T, Lv D, Zhang H. Modeling and experimental study of a linear power generator for road energy harvesting. *Journal of Renewable and Sustainable Energy*. 2017 Nov; 9(6):064702.

53. Karsilaya, A., Dessouky, S., & Papagiannakis, A.. Development of a Self-Powered Structural Health Monitoring System for Transportation Infrastructure. *Transportation Consortium of South-Central States (Tran-SET)*. 2018